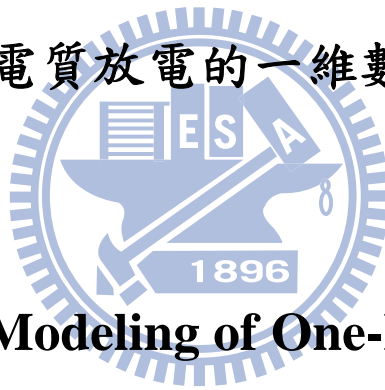


國立交通大學

機械工程學系

碩士論文

氮氣介電質放電的一維數值模擬



**Numerical Modeling of One-Dimensional  
Nitrogen Barrier Discharge**

研究生：王穎志

指導教授：吳宗信 博士

中華民國九十八年七月

氮氣介電質放電的一維數值模擬

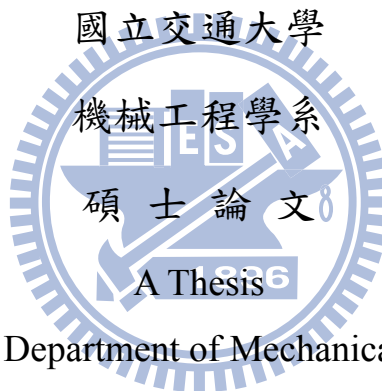
**Numerical Modeling of One-Dimensional  
Nitrogen Barrier Discharge**

研究生：王穎志

Student：Yin-Chin Wang

指導教授：吳宗信 博士

Advisor：Dr. Jong-Shinn Wu



Submitted to Department of Mechanical Engineering

College of Engineering

National Chiao Tung University

in Partial Fulfillment of the Requirements

for the Degree of

Master of Science

In

Mechanical Engineering

July 2009

Hsinchu, Tiwan

2009 年 7 月

# 氮氣介電質放電的一維數值模擬

學生： 王穎志

指導教授： 吳宗信 博士

交通大學 機械工程學系

## 摘要

本論文提出使用一維流體模型模擬氮氣介電質放電，使用平行化的流體模型來模擬純氮氣電漿。流體模型中所有的方程式都是使用牛頓-克雷洛夫-施瓦茲 (Newton-Krylov-Schwarz) 演算法離散，並搭配單一重疊的施瓦茲 preconditioner 和線性化矩陣的疊代方法 GMRES 來求解。

電子能量分布函數可從一套免費的軟體 BOLSIG 計算得出，計算所需的反應截面積需由使用者輸入，氮氣電漿中所有的傳輸係數和化學反應速率係數都可從電子能量分布函數算出，並且使用一個化學的模組來處理流體模型中化學反應的部分，氮氣電漿在本論文中，總共考慮八種粒子，分別是電子,  $N_2$ ,  $N_2(A^3)$ ,  $N_2(B^3)$ ,  $N_2(C^3)$ ,  $N_2(a^1)$ ,  $N_2^+$ ,  $N_4^+$ ，並考慮 30 個化學反應式，其中涵括了激發、電離、重組的反應。

討論氮氣電漿模擬的結果，並比較實驗與模擬得到的電流，可看出實驗與模擬的結果相符合，計算各帶電粒子吸收的能量可發現，離子較電子吸收了更多的能量。由模擬得到的密度分度可看出，本論文模擬的氮氣放電屬於 Townsend-like discharge。此外，也討論不同的介電質常數與不同放電區域大小對電漿的影響。

# Numerical Modeling of One-Dimensional Nitrogen Barrier Discharges

Student: Wang, Ying-Chih

Advisor: Dr. Wu, Jong-Shinn

Department of Mechanical Engineering

National Chiao-Tung University

## Abstract

A simulation of low temperature nitrogen dielectric barrier discharge (DBD) at atmosphere pressure is proposed in this thesis. The parallelized fluid modeling is used to simulate the pure nitrogen discharge. All of the model equations are discretized using fully coupled Newton-Krylov-Schwarz algorithm, in which the preconditioner and linear matrix solver are overlapping additive Schwarz method and Bi-CGSTb/GMRES scheme.

The transport coefficients of nitrogen plasma and chemical reaction rate are obtained from BOLSIG, which is a Boltzmann solver can evaluate electron energy distribution function by the user given cross sections. A chemistry module take care the reactions in fluid modeling, in which pure nitrogen chemistry in this thesis include 8 species,  $N_2$ ,  $N_2(A^3)$ ,  $N_2(B^3)$ ,  $N_2(C^3)$ ,  $N_2(a^1)$ ,  $N_2^+$ ,  $N_4^+$  and electron. 30 reaction channels are considered which include excitation, ionization and recombination

reactions.

The total currents of simulation and experiment are compared, and it reveals that the simulation result is corresponding to the experiment data. The power absorption is evaluated, and it shows that the absorbed power of ions is higher than the electron. According to the number densities of electron and positive ions simulated, it shows that the discharge is Townsend-like discharge. Furthermore, the influence of different dielectric permittivity and different discharge gap are discussed.



## 誌謝

在交大的求學過程，誠摯的感謝吳宗信教授在這兩年的諄諄教誨，您對學術的嚴謹和熱誠帶領著我們前進，並不時的為我們指引方向，在生活上非常照顧我們，在學習和生活上讓我獲益良多。同時也要感謝口試委員黃俊誠老師、江仲驊老師和徐振哲老師，謝謝您們在口試時提供的寶貴建議。另外特別感謝祭哥和邱哥兩位學長，不僅付出時間和心力教導我研究上的問題，同時也在linux作業系統的使用上對我悉心教導，也感謝昆模學長分享許多工作上的經驗談，與生活上的鼓勵。

感謝已畢業的學長姐們，貴哥、勁全哥、柳哥、阿志學長、玫琪學姊、阿龐學長等，也感謝實驗室的學長姐們，江學長、允民哥、富利學長、周學姊、孟樺學姊、雅茹學姊、正勤哥、豪哥等，與你們在一起相處的點點滴滴，一起在實驗室努力的時光，是我一生最寶貴的回憶。感謝同學古必、逸民和俊傑，在這兩年一同努力相互合作，也感謝學弟皓遠和小璋的大力幫忙，另外還有許多在生活或是學業上幫助我的人們或被不小心遺忘的朋友，在此也一併感謝，並祝福所有還在學的朋友們，能夠達到自己理想的目標。

最後要特別感謝我的家人，感謝他們對我的鼓勵與包容，在人生的旅途上我會更加努力向目標邁進。

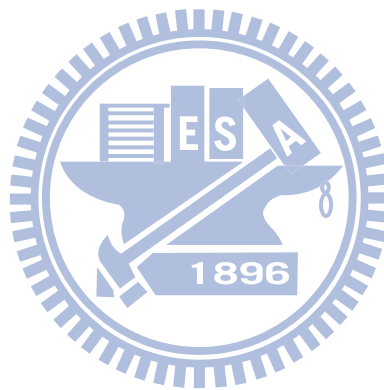
王穎志 謹誌

2009年7月於交通大學

# Table of Contents

摘要.....	I
Abstract.....	II
誌謝.....	IV
Table of Contents .....	V
List of Tables.....	VII
List of Figures .....	VIII
Nomenclature.....	X
Chapter 1 Introduction .....	1
1.1 Background and Motivation .....	1
1.2 Literature Survey .....	2
1.3 Specific Objectives of the Thesis.....	6
Chapter 2 Numerical Method.....	7
2.1 Fluid Modeling.....	7
2.1.1 Boltzmann Equation.....	7
2.1.2 Fluid Modeling Equations.....	8
2.1.3 Boundary Conditions.....	12
2.2 Numerical Methods.....	14
2.2.1 Nondimensionization.....	14
2.2.2 Finite-Difference Discretization of the Fluid Modeling Equations .	17
2.2.2.1 Temporal Discretization.....	17
2.2.2.2 Spatial Discretization .....	17
2.2.2.2.1 Diffusion Term.....	21
2.2.2.2.2 Drift (Convection) Term .....	21
2.2.3 Parallel Fully Implicit Newton-Krylov-Swartz-Algorithm .....	22
Chapter 3 Results and Discussions .....	24
3.1 Simulation Conditions .....	24
3.2 Plasma Chemistry .....	25
3.3 Results and Discussion .....	27
3.3.1 Conduction, Displacement and Total Currents .....	27
3.3.2 Power Absorptions and Light Emissions .....	29
3.3.3 Potential, Electron Temperature and Accumulated Charge .....	30

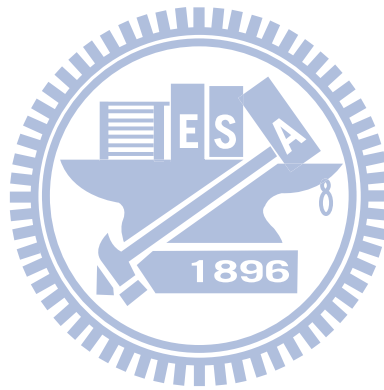
3.3.4	Charged Species.....	31
3.3.5	Neutral Species .....	33
3.3.6	Influence of Different Dielectric Permittivity.....	33
3.3.7	Influence of Different Gap Size.....	34
Chapter 4	Conclusions and Recommendation of Future Work.....	36
4.1	Conclusion Remarks .....	36
4.2	Recommendation of Future Work.....	37
Reference	.....	38





## List of Tables

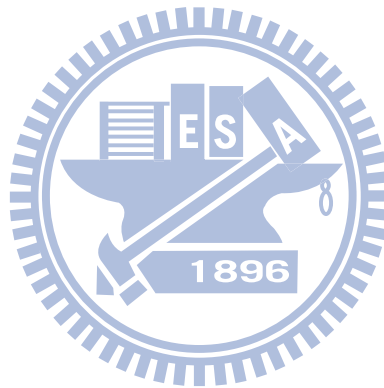
Table 1: The simulated condition of dielectric barrier discharge with pure nitrogen. .41	
Table 2: Nitrogen Plasma Chemistry .....	41
Table 3: The time average absorbed power of electron and ions. At the condition, the applied voltage (60 kHz), the gap size 1mm and dielectric thickness 1mm with permittivity 11.63.....	43
Table 4: The time average power of light emitted. At the condition, the applied voltage (60 kHz), the gap size 1mm and dielectric thickness 1mm with permittivity 11.63.....	43



## List of Figures

Figure 1: Sketch of 1D dielectric barrier discharge .....	44
Figure 2: Waveform of the applied voltage with the frequency 60 kHz which is measured from experiment .....	44
Figure 3: sketch of nitrogen plasma chemistry .....	45
Figure 4: The reaction rate coefficients of reaction channels, from No. (1) to (10), in nitrogen plasma .....	46
Figure 5: The reaction rate coefficients of reaction channels, from No. (11) to (15), in nitrogen plasma .....	46
Figure 6: Total current versus with time during one cycle of applied voltage (60 kHz) at the condition, the gap size 1mm and dielectric thickness 1mm with permittivity 11.63 .....	47
Figure 7: The gap voltage and the accumulated charge versus with time. ....	47
Figure 8: The displacement, conduction of charged species and the total during only cycle, Figure 8 a to Figure 8 h are shown in different time.....	51
Figure 9: The power absorption of charged species at the condition, the gap size 1mm and dielectric thickness 1mm with permittivity 11.63. ....	52
Figure 10: The power of the emitted light with different wavelength at the condition, the gap size 1mm and dielectric thickness 1mm with permittivity 11.63...52	52
Figure 11: The phase diagram of potential with gap size 1 mm and dielectric thickness 1 mm with permittivity 11.63 .....	53
Figure 12: The phase diagram of electron temperature with gap size 1 mm and dielectric thickness 1 mm with permittivity 11.63. ....	53
Figure 13: The phase diagram of electron number density with gap size 1 mm and dielectric thickness 1 mm with permittivity 11.63. ....	54
Figure 14: The phase diagram of $N_2^+$ number density with gap size 1 mm and dielectric thickness 1 mm with permittivity 11.63 .....	54
Figure 15: The phase diagram of $N_4^+$ number density with gap size 1 mm and dielectric thickness 1 mm with permittivity 11.63 .....	55
Figure 16: The phase diagram of $N_2(A^3)$ number density with gap size 1 mm and dielectric thickness 1 mm with permittivity 11.63 .....	55
Figure 17: The phase diagram of $N_2(a'^1)$ number density with gap size 1 mm and dielectric thickness 1 mm with permittivity 11.63 .....	56
Figure 18: The phase diagram of $N_2(B^3)$ number density with gap size 1 mm and dielectric thickness 1 mm with permittivity 11.63 .....	56
Figure 19: The phase diagram of $N_2(C^3)$ number density with gap size 1 mm and	

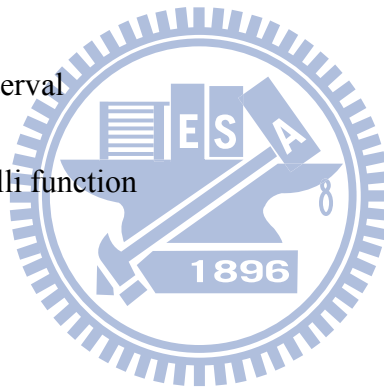
dielectric thickness 1 mm with permittivity 11.63 .....	57
Figure 20: The source terms of electron continuity equation source terms shows in each reaction channels. ....	59
Figure 21: The sketches of potential, number density and electron temperature at different time, which from <i>Figure 21 a</i> to <i>Figure 21 e</i> , with the frequency of applied voltage 60 kHz. ....	64
Figure 22: The total current during one cycle with the same applied voltage, gap size 1mm and different dielectric permittivity from 9 to 12.....	65
Figure 23: The accumulated charge at left dielectric surface with different dielectric permittivity, and the gap size is 1 mm with 60 kHz applied voltage.....	65
Figure 24: The total current during one cycle with the same applied voltage, dielectric permittivity 11.63 and gap size various from 0.5 mm to 2 mm.....	66
Figure 25: The accumulated charge during one cycle with the same applied voltage, dielectric permittivity 11.63 and gap size various from 0.5 mm to 2 mm..	66



## Nomenclature

$m$	mass
$P$	pressure
$q$	charge
$k_B$	the Boltzmann constant
$n$	number density
$l$	thickness of dielectric barrier
$L$	gap size of discharge region
$\Gamma$	particle flux
$v_{th}$	thermal velocity
$\gamma$	factor of secondary electron emission
$S$	source and sink of continuity equation
$T_e$	electron temperature
$\varepsilon$	energy loss for inelastic electron collision
$\phi$	potential
$\varepsilon_0$	vacuum permittivity
$\varepsilon_d$	dielectric permittivity
$E$	electric field
$f$	electron energy distribution function

$\sigma$	cross section
$k$	reaction rate coefficient
$\mu$	mobility
$D$	diffusivity
$\nu_m$	momentum exchange collision frequency between electron and background neutral particles
$\alpha$	polarizability
$\Delta x$	space interval
$\Delta t$	time interval
$B$	Bernoulli function



# Chapter 1 Introduction

## 1.1 Background and Motivation

Plasma is one of the substance phases, in which some electrons are free rather than be bounded by atoms or molecules, it means that some of the electron and ion species in the gas can move independently. With sufficient energy to overcome the electron bonding energy, which is called *ionize*, the evaporating of atoms or molecules has phase transition to become plasma. Furthermore, with increasing the temperature, more and more electrons are stripped until all the atoms or molecules are ionized. It's called *fully ionized plasma*.

Dielectric barrier discharge at atmospheric pressure has been widely applied in material processing since the early days, due to its ability to ash, clean or oxide without heating to high temperature, there are several applications such as surface treatment, photoresist ashing, striping polymer films and plasma display cells. The applications of plasma not only produce the value to billions dollars, but also improve human life. Since the nitrogen plasma applies well, but unfortunately the physic inside the nitrogen plasma is incomplete by using purely experiments, the numerical simulation can help us to study the nitrogen plasma.

Because of the movements of positive and negative species are not only affected by the density gradient, but also influenced by electric field and magnetic field, the properties of plasma are changed by those things. Furthermore, the chemistry of the nitrogen plasma, which including dissociation, excitation, ionization and recombination, is complex. The light intensity and electrical characteristics are usually measured from experiments, but it's difficult to measure all the properties in the nitrogen plasma through experiments. Therefore, the numerical simulation plays an important role for the investigation of nitrogen plasma.

## 1.2 Literature Survey

Numerical simulations in plasma are generally distinguished by Kinetic models, Fluid models and Hybrid models. Kinetic models solve Boltzmann equation by direct integration or statistical techniques, such as Particle in Cell Monte Carlo Method. Fluid models solve the species continuity, moment or energy equations of Boltzmann equation. The transport coefficients and reaction rate of electron-molecule reaction can be evaluated by electron energy distribution function (EEDF).

The 1D fluid models, which are solving continuity equations and Poisson equation, for simulating dielectric barrier discharge have been studied by several authors, and the discharge gases are pure nitrogen<sup>[1],[15],[16]</sup>, the mixture of nitrogen

and oxygen <sup>[10],[16]</sup>, and the mixture of nitrogen and helium <sup>[3],[14]</sup>.

The influence of electron emission from dielectric barrier and surface recombination is studied [Y. B. Golubovskii *et al.*, 2005]. The fluid model for simulating nitrogen barrier discharge at atmosphere pressure is presented, which the sinusoidal applied voltage at amplitude 15 kV and frequency 1 kHz, and the nitrogen chemistry contains 5 species and 8 reaction channels. The simulation shows that the nitrogen discharge may be Townsend discharge, and the current density are compare between simulation and experiment with different frequency, which varies from 1 kHz to 35 kHz.

The glow dielectric barrier discharge (GDBD) with nitrogen and helium gas is studied, and it shows that the Townsend discharge is changing into glow discharge during the current increase [F. Massines *et al.*, 2003]. The numerical results are compared with the emission spectroscopy measured by experiment.

A nonthermal atmospheric dielectric barrier discharge in nitrogen and helium is presented [X. T. Deng and M. G. Kong, 2004], the chemistry of nitrogen includes 11 species and 17 reaction channels. According to the simulation, it shows that most electrons, which are produced in the bulk, are trapped and can not reach the electrode while the excitation frequency is high. This observation reveals the importance of the balance about the applied voltage and the voltage between the dielectric barriers.



The nitrogen with small admixtures of oxygen barrier discharge at frequency 6.95 kHz is studied [R. Brandenburg *et al.*, 2005]. The electric characteristics with different external admixture of O<sub>2</sub> and the spectroscopic diagnostics are measured from experiment, and the discharge current and displacement current are compared with numerical and experiment results. The transition to the filamentary mode and the discharge mechanism are discussed, this transition starts from less of oxygen (about 450 ppm) to the micro-discharges, which are generated at higher admixtures of O<sub>2</sub> (about 1000 ppm).

The 1D fluid model for pure nitrogen atmospheric pressure plasma is studied [Y. H. Choi *et al.*, 2006]. The influences of different driving frequencies and voltage amplitudes are discussed while the amplitude of sinusoidal applied voltage is 6-10 kV and frequency changes from 10 to 20 kHz. The simulation of pure nitrogen barrier discharge and the nitrogen with oxygen are presented, and the influence of different content of oxygen and different secondary electron coefficient are discussed.

The coupled electro-dynamic and kinetic model of pure nitrogen dielectric barrier discharge at high frequency (130 kHz) is presented [E. Panousis *et al.*, 2007], and there are 45 vibration states of nitrogen and its excited state considered in the plasma chemistry. The discharge's efficiency of species is calculated, and the electrical and optical diagnostics are compared between experimental data and

numerical results.

The 2D fluid models which are solving continuity equations and Poisson equation, Cartesian or axisymmetric axis, of dielectric barrier discharge at atmospheric pressure have been studied by many authors <sup>[5],[8],[12]</sup>.

Two dimensional Cartesian model is presented [P. Zhang *et al.*, 2006], and the simulation of the atmospheric pressure glow discharge of helium with a few nitrogen impurities is simulated. The governing equations are continuity equation of species with drift-diffusion approximation and Poisson equation, and properties of species are based on the local field approximation. The numerical result shows that the penning ionization is the dominant mechanism to generating electron, and the increasing the frequency of applied voltage lead to the transition from filamentary discharge to uniform glow discharge.

Two dimensional cylindrically symmetric simulation of nitrogen with a few oxygen is studied [V. A. Maiorov *et al.*, 2007], and the discussion are focused on the stability issues of Townsend, glow and multi-peak mode and the effect due to the added oxygen density. It proves that the lower permittivity barriers has widening stability region.

The influence of filamentary mode of two dimensional axisymmetric model of the dielectric barrier discharge is studied [L. Papageorghiou *et al.*, 2009], and the gas

is nitrogen at atmospheric pressure and the gap size is 1 *mm*, and the numerical result shows that the development of discharge are two phases. The first phase is the propagation and formation of the ionizing wave, and second, the surface streamer is formed on dielectric surface.

### **1.3 Specific Objectives of the Thesis**

Since it's difficult to measure all the properties of the plasma, the numerical simulation is used to study the oxygen plasma. Therefore, the specific objectives of this thesis are summarized as follow,

1. To simulate the 1-D nitrogen dielectric barrier discharge at atmospheric pressure and compare the numerical result with experiment data.
2. To discuss the plasma chemistry with nitrogen gas and its physics of dielectric barrier discharge.
3. To study the influences of dielectric barrier discharge with different gap size and different dielectric permittivity.

## Chapter 2 Numerical Method

### 2.1 Fluid Modeling

#### 2.1.1 Boltzmann Equation

According to kinetic theory, the plasma can be described by a distribution function  $f(\mathbf{r}, \mathbf{v}, t)$ , which satisfies the Boltzmann equation (Vlasov equation), at location  $\mathbf{r}$ , velocity  $\mathbf{v}$  and time  $t$ ,

$$\frac{\partial}{\partial t} f(\mathbf{r}, \mathbf{v}, t) + \mathbf{v} \cdot \nabla_{\mathbf{r}} f(\mathbf{r}, \mathbf{v}, t) + \frac{q}{m} (\mathbf{E} + \mathbf{v} \times \mathbf{B}) \cdot \frac{\partial f(\mathbf{r}, \mathbf{v}, t)}{\partial \mathbf{v}} = \left( \frac{\partial f(\mathbf{r}, \mathbf{v}, t)}{\partial t} \right)_c$$

, where  $q$  is charge,  $m$  is mass, and the term in right hand side is due to collision. If we take the first three velocity moments of  $f(\mathbf{r}, \mathbf{v}, t)$ , the spatial and temporal distribution of density, flux, and temperature can be described as

$$n(\mathbf{r}, t) = \int f(\mathbf{r}, \mathbf{v}, t) d^3 \mathbf{v}$$

$$\Gamma(\mathbf{r}, t) = \int \mathbf{v} f(\mathbf{r}, \mathbf{v}, t) d^3 \mathbf{v}$$

$$\frac{3}{2} k_B T(\mathbf{r}, t) = \frac{m \int v^2 f(\mathbf{r}, \mathbf{v}, t) d^3 \mathbf{v}}{2 \int f(\mathbf{r}, \mathbf{v}, t) d^3 \mathbf{v}}$$

Similarity, we take the three previous integrations of Boltzmann equation to get the continuity equation, momentum equation and energy equation, these equations can be written as,

$$\frac{\partial}{\partial t}n + \nabla \cdot (nv) = S$$

$$mn \left[ \frac{\partial v}{\partial t} + (v \cdot \nabla)u \right] = qn(E + v \times B) - \nabla \cdot P + M$$

$$\frac{\partial}{\partial t}(nC_v T) + \nabla \cdot (nC_v T) = -\nabla \cdot q - p \nabla \cdot v + E$$

, where  $S$  is the source and sink of the continuity equation,  $M$  is the momentum transfer of the species,  $E$  is the energy gain and loss of the species,  $C_v$  is the specific heat capacity.

## 2.1.2 Fluid Modeling Equations

In general fluid modeling, the densities of electron, ion and neutral species are function of time and space, which are calculating from the species continuity equations, species momentum equations and species energy equations. Further, the self-consistent model includes the Poisson's equation.

Transport coefficients, mobility and diffusivity, are used instead of solving species momentum equations, and ignoring the ionic and neutral species energy equations because of the non-thermal plasma is considered. Therefore, only species continuity equations, electron energy equation and Poisson's equation are solved [C.-T. Hung *et al.*, unpublished].

The general continuity equation for ion species can be written as

$$\frac{\partial n_p}{\partial t} + \frac{\partial \Gamma_p}{\partial x} = \sum_{i=1}^{r_p} S_{pi}, \quad p = 1, 2, \dots, k$$

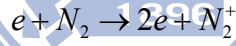
, where  $n_p$  is the number density of ion species  $p$ ,  $k$  is the number of ion species,  $r_p$  is the number of reaction channels that involve the creation and destruction of ion species  $p$ , and  $\vec{\Gamma}_p$  is the ion particle flux that is expressed as, base on the drift-diffusion approximation,

$$\Gamma_p = \text{sign}(q_p)\mu_p n_p E - D_p \frac{\partial n_p}{\partial x}$$

, where  $q_p$ ,  $\mu_p$ , and  $D_p$  are the ion charge, the ion mobility, and the ion diffusivity of the species  $p$ . The electric field  $E$  can be calculated by the potential  $\phi$  as

$$E = -\frac{\partial \phi}{\partial x}$$

The source term  $S$  is calculated from the chemistry reactions, for example, there is a reaction channel which reaction rate is  $k_i$  as following,



Therefore, the source term of  $N_2^+$  can be written as,

$$S_i = k_i n_e n_{N_2}$$

The continuity equation for electron species  $e$  can be written as

$$\frac{\partial n_e}{\partial t} + \frac{\partial \Gamma_e}{\partial x} = \sum_{i=1}^{r_e} S_{ei}$$

, where  $n_e$  is number density of electron,  $r_e$  is the number of reaction channels that involve the creation and destruction of electron, and  $\vec{\Gamma}_e$  is the electron particle flux that is expressed as, base on the drift-diffusion approximation,

$$\Gamma_e = \text{sign}(q_e)\mu_e n_e E - D_e \frac{\partial n_e}{\partial x}$$

, where  $\mu_e$  and  $D_e$  are the electron mobility and electron diffusivity.

The continuity equation for neutral species can be written as

$$\frac{\partial n_{uc}}{\partial t} + \frac{\partial \Gamma_{uc}}{\partial x} = \sum_{i=1}^{r_{uc}} S_{uc,i}, \quad uc = 1, 2, \dots, k$$

, where  $n_{uc}$  is number density of electron,  $r_{uc}$  is the number of reaction channels that involve the creation and destruction of neutral species  $uc$ , and  $\vec{\Gamma}_e$  is the particle flux only considering the diffusion effect,

$$\Gamma_{uc} = -D_{uc} \frac{\partial n_{uc}}{\partial x}$$

, where  $D_{uc}$  is the diffusivity of neutral species  $uc$ .

The electron energy density equation can be written as,

$$\frac{\partial n_\varepsilon}{\partial t} + \frac{\partial \Gamma_\varepsilon}{\partial x} = -e\Gamma_e E - \sum_{i=1}^{S_\varepsilon} \varepsilon_i S_i + 3 \frac{m_e}{M} n_e k_B \nu_m (T_e - T_g)$$

, where  $T_e$  is the electron temperature,  $T_g$  is the background gas temperature,  $\varepsilon_i$  is the energy loss for  $i^{th}$  inelastic electron collision,  $k_B$  is Boltzmann constant, and  $\nu_m$  is the momentum exchange collision frequency between electron and background neutral particles.  $n_\varepsilon$  is the electron energy density which is defined as

$$n_\varepsilon = \frac{3}{2} n_e k_B T_e$$

The electron energy density flux  $\vec{\Gamma}_\varepsilon$  is

$$\Gamma_\varepsilon = \frac{5}{2} k_B T_e \Gamma_e - \frac{5}{2} \frac{n_e k_B T_e}{m_e \nu_m} \nabla(k_B T_e)$$

Poisson's equation can be written as,

$$\frac{\partial^2 \phi}{\partial x^2} = -\frac{1}{\varepsilon_0} \left( \sum_{i=1}^k (\text{sign}) q_i n_i - e n_e \right)$$

, where  $\varepsilon_0$  is the vacuum permittivity.

A independent chemistry module is used for deal with the source terms  $S_{p,e,uc}$  and transport coefficients  $D_{p,e,uc}$  and  $\mu_{p,e}$  in all the continuity equations. User can change reacting species and chemical reactions by inputting a description of the species properties, reaction channels and related rate coefficients.

By chemical kinetic description, the source terms are evaluated from reaction rate coefficients  $k$  which can be obtained by integrating cross sections with the electron energy density function (EEDF). A Boltzmann solver, such as BOLSIG<sup>[4]</sup> which is a public available freeware, can calculate the EEDF  $f$  by the user giving reaction channels and cross sections  $\sigma_i$ .

Therefore, the reaction rate coefficient of  $i^{\text{th}}$  reactions can be calculated as,

$$k_i(T) = \int_0^{\infty} f \cdot v \cdot \sigma_i \cdot 4\pi v^2 dv$$

Since Einstein relation, the transport coefficients of electron is written as,

$$\mu_e = \frac{|q_e|}{m_e \nu_m}$$

$$D_e = \frac{k_B T_e}{m_e \nu_m}$$

, where  $m_e$  is the mass of electron and  $\nu_m$  is the electron momentum transfer collision frequency.

The mobility of ion species  $p$  is



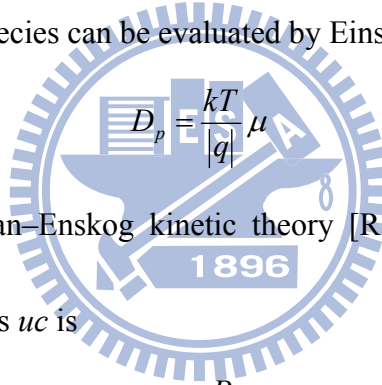
$$\mu_p = \frac{P_{total}}{\sum_{i=1}^l \left( \frac{P_i}{\mu_{i,p}} \right)}$$

, where

$$\mu_{i,p} = 0.514 \frac{T}{P_{total} \sqrt{m^* \alpha_i}}$$

,  $P$  is the pressure, and  $l$  is the number of all the species which including neutral and ionic species,  $\alpha_i$  is polarizability of the species  $i$ , and  $m^*$  is the reduced mass which calculated from the mass of species  $i$  and  $p$ .

The mobility of ion species can be evaluated by Einstein relation as,



$$D_p = \frac{kT}{|q|} \mu$$

According to Chapman–Enskog kinetic theory [R. B. Bird *et al.*, 1960], the diffusivity of neutral species  $uc$  is

$$D_{uc} = \frac{P_{total}}{\sum_{i=1}^l \frac{P_i}{D_{i,uc}}}$$

, where

$$D_{i,uc} = 0.0018583 \sqrt{T^3 \left( \frac{1}{M_i} + \frac{1}{M_{uc}} \right)} \frac{1}{P \sigma_{i,uc}^2 \Omega_{i,uc}}$$

,  $M$  is molecule weight,  $\sigma$  is characteristic diameter, and  $\Omega$  is collisional integral.

### 2.1.3 Boundary Conditions

The sketch of one dimensional dielectric barrier discharge is shown in *Figure 1*,

and the governing equations, species continuity equations, electron energy equation and Poisson's equation, are solved in this thesis. According to plasma kinetic description, the boundary condition of continuity equation at dielectric surface for ion species  $p$  is

$$\Gamma_p = \frac{1}{4} n_p v_{th,p} - \text{sign}(q_p) \mu_p n_p \frac{\partial \phi}{\partial x} - D_p \frac{\partial^2 n_p}{\partial x^2}$$

, where  $v_{th,p}$  is the thermal velocity which is defined as

$$v_{th,p} = \sqrt{\frac{8k_B T_p}{\pi m_p}}$$

The boundary condition of continuity equation for electron  $e$  is

$$\Gamma_e = \frac{1}{4} n_e v_{th,e} + \mu_e n_e \frac{\partial \phi}{\partial x} - D_e \frac{\partial^2 n_e}{\partial x^2} - \gamma \Gamma_p$$

, where  $\gamma$  is the factor of secondary electron emission caused by ion bombarding the wall, and  $v_{th,e}$  is the thermal velocity which is defined as

$$v_{th,e} = \sqrt{\frac{8k_B T_e}{\pi m_e}}$$

The boundary condition of continuity equation for neutral species  $uc$  is the Neumann boundary, since no surface reactions are considered in this thesis.

$$\vec{\Gamma}_{uc} = 0$$

The boundary condition of Poisson's equation at dielectric surface is

$$\left\{ \begin{array}{l} \phi = \phi(t) \quad , at \quad x = 0 \\ \varepsilon_0 \frac{\partial \phi}{\partial x} - \varepsilon_d \frac{\partial \phi_d}{\partial x} = -\sigma_s \quad , at \quad x = l \\ \varepsilon_d \frac{\partial \phi_d}{\partial x} - \varepsilon_0 \frac{\partial \phi}{\partial x} = -\sigma_s \quad , at \quad x = l + L \\ \phi = 0 \quad , at \quad x = 2l + L \end{array} \right.$$

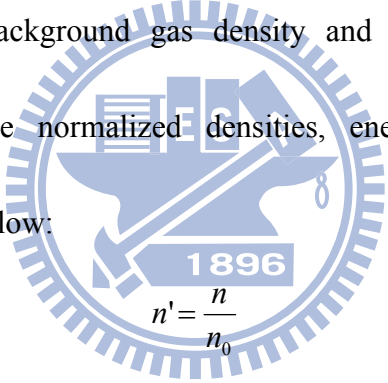
The boundary condition of the electron energy density at dielectric surface is

$$\Gamma_\varepsilon = 2k_B T_e \Gamma_e$$

## 2.2 Numerical Methods

### 2.2.1 Nondimensionization

Let  $n_0$  denote the background gas density and  $T_0$  is normalized electron temperature factor, so the normalized densities, energy density and electron temperature are listed as follow:



$$n' = \frac{n}{n_0}$$

$$n_\varepsilon' = \frac{n_\varepsilon}{n_0 k_B T_0}$$

$$T_e' = \frac{T_e}{T_0}$$

The normalized time and length are

$$t' = \frac{u_0}{\lambda} t$$

$$x' = \frac{x}{\lambda}$$

, where the character length is

$$\lambda = \frac{1}{n_0 \sigma_p}$$

The normalized velocity is

$$u_p' = \frac{u_p}{u_0}$$

$$u_e' = \frac{u_e}{u_0}$$

, where  $u_0$  is

$$u_0 = \sqrt{\frac{k_B T_0}{m_p}}$$

The normalized potential, source term and energy are

$$\phi' = \frac{e\phi}{k_B T_0}$$

$$S_e' = \frac{S_e}{n_0 u_0 / \lambda}$$

$$\varepsilon' = \frac{e}{k_B T_0} \varepsilon$$

The dimensionless diffusivity and mobility are

$$D' = \frac{D}{\lambda u_0}$$

$$\mu' = \frac{m_p u_0}{e \lambda} \mu$$

Therefore, the continuity equations can be written as,

$$\frac{n_0 u_0}{\lambda} \frac{\partial n'_{e,p,uc}}{\partial t'} + \frac{1}{\lambda} \frac{\partial (n_0 u_0 \Gamma'_{e,p,uc})}{\partial x'} = \frac{n_0 u_0}{\lambda} S'_{e,p,uc}$$

$$\frac{\partial n'_{e,p,uc}}{\partial t'} + \frac{\partial (\Gamma'_{e,p,uc})}{\partial x'} = S'_{e,p,uc}$$

, where the particles flux terms are

$$\vec{\Gamma}'_p = -\text{sign}(q_p) \mu'_p n'_p \frac{\partial \phi'}{\partial x'} - D'_p \frac{\partial n'_p}{\partial x'}$$

$$\vec{\Gamma}'_e = -\text{sign}(q_e) \mu'_e n'_e \frac{\partial \phi'}{\partial x'} - D'_e \frac{\partial n'_e}{\partial x'}$$

$$\vec{\Gamma}'_{uc} = -D'_{uc} \frac{\partial n'_{uc}}{\partial x'}$$

The dimensionless electron energy equation is

$$\frac{u_0}{\lambda} n_0 k_B T_0 \frac{\partial n'_\varepsilon}{\partial t'} + \frac{1}{\lambda} n_0 u_0 k_B T_0 \frac{\partial \Gamma'_\varepsilon}{\partial x'} = e \left( n_0 u_0 \vec{\Gamma}'_e \left( \frac{k_B T_e}{e} \frac{1}{\lambda} \frac{\partial \phi'}{\partial x'} \right) - \frac{k_B T_e}{e} \varepsilon' \left( \frac{n_0 u_0}{\lambda} S'_e \right) \right)$$

$$\frac{\partial n'_\varepsilon}{\partial t'} + \frac{\partial \Gamma'_\varepsilon}{\partial x'} = -\vec{\Gamma}'_e \cdot \vec{E}' - \frac{\varepsilon' S'_e}{e}$$

$$\frac{\partial n'_\varepsilon}{\partial t'} + \frac{\partial \Gamma'_\varepsilon}{\partial x'} = S'_\varepsilon$$

The dimensionless Poisson's equation is

$$\frac{1}{\lambda^2} \frac{\partial^2 \left( \frac{k_B T_0}{e} \phi' \right)}{\partial x'^2} = -\frac{en_0}{\varepsilon_0} \left( \sum_{i=1}^k (\text{sign}) n'_i - n'_e \right)$$

$$\frac{\partial^2 \phi'}{\partial x'^2} = -\frac{\lambda^2 e^2 n_0}{\varepsilon_0 k_B T_0} \left( \sum_{i=1}^k (\text{sign}) n'_i - n'_e \right)$$

$$\frac{\partial^2 \phi'}{\partial x'^2} = -\frac{1}{\varepsilon'_0} \left( \sum_{i=1}^k (\text{sign}) n'_i - n'_e \right)$$

, where

$$\varepsilon'_0 = \frac{\varepsilon_0 u_0^2 m_p}{\lambda^2 e^2 n_0}$$

## 2.2.2 Finite-Difference Discretization of the Fluid Modeling

### Equations

#### 2.2.2.1 Temporal Discretization

In this thesis, all the fluid modeling equations, species continuity equations, electron energy equation and Poisson's equation, are discretized through using finite-difference scheme. The first-order fully-implicit backward Euler scheme is used for temporal discretization. The fully-couple equations, one dimensional species continuity equations, electron energy equation and Poisson's equation, are written as,

$$\frac{n_{p,e,uc}^{t+\Delta t} - n_{p,e,uc}^t}{\Delta t} + \left( \frac{\partial \Gamma_{p,e,uc}}{\partial x'} \right)^{t+\Delta t} = (S_{p,e,uc})^{t+\Delta t}$$

$$\frac{n_{\varepsilon}^{t+\Delta t} - n_{\varepsilon}^t}{\Delta t} + \left( \frac{\partial \Gamma_{\varepsilon}}{\partial x} \right)^{t+\Delta t} = (S_{\varepsilon})^{t+\Delta t}$$

$$\left( \frac{\partial^2 \phi}{\partial x^2} \right)^{t+\Delta t} = -\frac{1}{\varepsilon_0} \left( \sum_{i=1}^k (\text{sign}) n_i - n_e \right)^{t+\Delta t}$$

#### 2.2.2.2 Spatial Discretization

The continuity equations of each species and electron energy equation can be expressed as,

$$\frac{n_{p,e}^{t+\Delta t} - n_{p,e}^t}{\Delta t} + \frac{(\Gamma_{p,e})_{i+1/2}^{t+\Delta t} - (\Gamma_{p,e})_{i-1/2}^{t+\Delta t}}{\Delta x} = (S_{p,e})^{t+\Delta t}$$

$$\frac{n_{uc}^{t+\Delta t} - n_{uc}^t}{\Delta t} + \frac{(\Gamma_{uc})_{i+1/2}^{t+\Delta t} - (\Gamma_{uc})_{i-1/2}^{t+\Delta t}}{\Delta x} = (S_{uc})^{t+\Delta t}$$

$$\frac{n_{\varepsilon}^{t+\Delta t} - n_{\varepsilon}^t}{\Delta t} + \frac{(\Gamma_{\varepsilon})_{i+1/2}^{t+\Delta t} - (\Gamma_{\varepsilon})_{i-1/2}^{t+\Delta t}}{\Delta x} = (S_{\varepsilon})^{t+\Delta t}$$

The ion and electron flux is changed for different positions. The diffusion term is dominated in the “bulk”, where the electric field is vanished because of Debye shielding. In the “sheath”, where the plasma potential drives the changes of ionic species and electron, the convection term is dominated. In order to express the regional difference, continuity equation can be discretized by the numerical discretization scheme, called Scharfetter-Gummel Scheme. This scheme is employed for spatial discretization of convection dominated problems, which are ion and electron continuity equations, then the ion flux can be written as,

$$\Gamma_{p,i+1/2} = -D_{p,i+1/2} \frac{\partial n_p}{\partial x} - \mu_{p,i+1/2} \frac{\partial \phi_p}{\partial x} n_p$$

, where is a first-order differential equation of electron flux, We change the variable from position to potential by chain rule,

$$\frac{\partial \phi}{\partial x} \frac{\partial}{\partial \phi} n_p + \frac{\mu_{p,i+1/2}}{D_{p,i+1/2}} \frac{\partial \phi}{\partial x} n_p = - \frac{\Gamma_{p,i+1/2}}{D_{p,i+1/2}}$$

, which assume that  $\frac{\partial \phi}{\partial x}$  is independent to potential,

$$\frac{\partial}{\partial \phi} n_p + \frac{\mu_{p,i+1/2}}{D_{p,i+1/2}} n_p = - \frac{\Gamma_{p,i+1/2}}{D_{p,i+1/2} \frac{\partial \phi}{\partial x}}$$

The analytic solution of the first-order differential equation is

$$n_p(\phi) = Ce^{\frac{\mu_{p,i+1/2}\phi}{D_{p,i+1/2}}} - \frac{\Gamma_{p,i+1/2}}{\mu_{p,i+1/2}} \frac{\partial \phi}{\partial x}$$

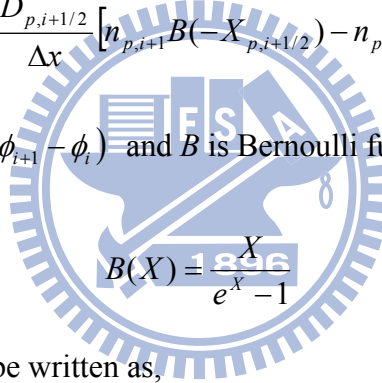
Consider the boundary condition  $n_{p,i} = n_{p,i}(\phi_i)$  and  $n_{p,i+1} = n_{p,i+1}(\phi_{i+1})$ , the  $C$  and  $\Gamma_{p,i+1/2}$  can be determined as,

$$C = \frac{n_{p,i} - n_{p,i+1}}{e^{-\frac{\mu_{p,i+1/2}\phi_i}{D_{p,i+1/2}}} - e^{-\frac{\mu_{p,i+1/2}\phi_{i+1}}{D_{p,i+1/2}}}}$$

$$\Gamma_{p,i+1/2} = -\frac{D_{p,i+1/2}}{\Delta x} \left[ \begin{array}{cc} -\frac{\mu_{p,i+1/2}}{D_{p,i+1/2}}(\phi_{i+1} - \phi_i) & -\frac{\mu_{p,i+1/2}}{D_{p,i+1/2}}(\phi_{i+1} - \phi_i) \\ \frac{\mu_{p,i+1/2}}{D_{p,i+1/2}}(\phi_{i+1} - \phi_i) & -1 \end{array} n_{p,i+1} - \begin{array}{cc} -\frac{\mu_{p,i+1/2}}{D_{p,i+1/2}}(\phi_{i+1} - \phi_i) & -\frac{\mu_{p,i+1/2}}{D_{p,i+1/2}}(\phi_{i+1} - \phi_i) \\ \frac{\mu_{p,i+1/2}}{D_{p,i+1/2}}(\phi_{i+1} - \phi_i) & -1 \end{array} n_{p,i} \right]$$

$$\Gamma_{p,i+1/2} = -\frac{D_{p,i+1/2}}{\Delta x} [n_{p,i+1} B(-X_{p,i+1/2}) - n_{p,i} B(X_{p,i+1/2})]$$

, where  $X_{p,i+1/2} = \frac{\mu_{p,i+1/2}}{D_{p,i+1/2}}(\phi_{i+1} - \phi_i)$  and  $B$  is Bernoulli function,



$$B(X) = \frac{X}{e^X - 1}$$

The electron flux can be written as,

$$\Gamma_e = -\frac{1}{m_e \nu_m} \frac{\partial(n_e k_B T_e)}{\partial x} - \frac{q_e n_e}{m_e \nu_m} \bar{E}$$

$$= -\frac{n_e}{m_e \nu_m} \frac{\partial(k_B T_e)}{\partial x} - \frac{k_B T_e}{m_e \nu_m} \frac{\partial n_e}{\partial x} + \frac{q_e n_e}{m_e \nu_m} \frac{\partial \phi}{\partial x}$$

The first-order differential equation can be written as,

$$\frac{k_B T_e}{m_e \nu_m} \frac{\partial n_e}{\partial x} + \left( \frac{1}{m_e \nu_m} \frac{\partial(k_B T_e)}{\partial x} - \frac{q_e}{m_e \nu_m} \frac{\partial \phi}{\partial x} \right) n_e = -\Gamma_e$$

$$\frac{\partial n_e}{\partial x} + \left( \frac{1}{k_B T_e} \frac{\partial(k_B T_e)}{\partial x} - \frac{q_e}{k_B T_e} \frac{\partial \phi}{\partial x} \right) n_e = -\frac{\Gamma_e}{\frac{k_B T_e}{m_e \nu_m}}$$

We change the variable from position to potential by chain rule, and assume that



$\frac{\partial \phi}{\partial x}$  is independent to potential,

$$\frac{\partial n_e}{\partial \phi} + \left( \frac{1}{k_B T_e} \frac{\partial(k_B T_e)}{\partial x} - \frac{q_e}{k_B T_e} \frac{\partial \phi}{\partial x} \right) \frac{1}{\frac{\partial \phi}{\partial x}} n_e = - \frac{\Gamma_e}{k_B T_e} \frac{\partial \phi}{m_e \nu_m \partial x}$$

$$\frac{\partial n_e}{\partial \phi} + a n_e = -b$$

, where  $a$  and  $b$  is

$$a = \left( \frac{1}{k_B T_e} \frac{\partial(k_B T_e)}{\partial x} - \frac{q_e}{k_B T_e} \frac{\partial \phi}{\partial x} \right) \frac{1}{\frac{\partial \phi}{\partial x}}$$

$$b = \frac{\Gamma_e}{k_B T_e} \frac{\partial \phi}{m_e \nu_m \partial x}$$

The solution of electron density is

$$n_e(\phi) = C e^{-a\phi} + \frac{b}{a}$$

Consider the boundary condition  $n_{e,i} = n_{e,i}(\phi_i)$  and  $n_{e,i+1} = n_{e,i+1}(\phi_{i+1})$ , the  $C$

and  $\Gamma_{e,i+1/2}$  can be determined as,

$$C = \frac{n_{e,i+1} - n_{e,i}}{e^{-a\phi_{i+1}} - e^{-a\phi_i}}$$

$$\Gamma_{e,i+1/2} = - \frac{1}{\Delta x} \frac{k_B T_e}{m_e \nu_m} \left[ n_{e,i+1} B(-X_{e,i+1/2}) - n_{e,i} B(X_{e,i+1/2}) \right]$$

, where

$$X_{e,i+1/2} = \left[ \frac{1}{k_B T_{e,i+1/2}} \frac{\partial(k_B T_e)}{\partial x} \right]_{i+1/2} - \frac{q_e}{k_B T_{e,i+1/2}} \left( \frac{\partial \phi}{\partial x} \right)_{i+1/2} \right] \frac{1}{\left( \frac{\partial \phi}{\partial x} \right)_{i+1/2}} (\phi_{i+1} - \phi_i)$$

$$= \left( \frac{1}{k_B T_{e,i+1/2}} \frac{k_B (T_{e,i+1} - T_{e,i})}{\phi_{i+1} - \phi_i} - \frac{q_e}{k_B T_{e,i+1/2}} \right) (\phi_{i+1} - \phi_i)$$

$$= \frac{T_{e,i+1} - T_{e,i}}{T_{e,i+1/2}} - \frac{q_e (\phi_{i+1} - \phi_i)}{k_B T_{e,i+1/2}}$$

### 2.2.2.2.1 Diffusion Term

The ion and electron flux terms of continuity equations, which are convection dominated, are already expressed as Scharfetter-Gummel Scheme. The other equations, neutral continuity equation, electron energy equation and Poisson's equation, are discretized by centered finite difference scheme, therefore the diffusion terms of neutral continuity equation can be written as,

$$-D_{uc} \frac{n_{uc,i+1} - 2n_{uc,i} + n_{uc,i-1}}{\Delta x^2}$$

The diffusion term of electron energy equation is

$$\frac{5}{2} \frac{k_B}{m_e v_m} \frac{n_{e,i+1/2} T_{e,i+1/2} (k_B T_{e,i+1}) - (n_{e,i+1/2} T_{e,i+1/2} + n_{e,i-1/2} T_{e,i-1/2}) (k_B T_{e,i}) + n_{e,i-1/2} T_{e,i-1/2} (k_B T_{e,i-1})}{(\Delta x)^2}$$

The diffusion term of Poisson equation can be written as

$$\frac{\phi_{i+1} - 2\phi_i + \phi_{i-1}}{(\Delta x)^2}$$

### 2.2.2.2.2 Drift (Convection) Term

The convection term of energy equation can be written as

$$\frac{5}{2} \frac{T_{e,i+1/2} \Gamma_{e,i+1/2} - T_{e,i-1/2} \Gamma_{e,i-1/2}}{\Delta x}$$

Finally, all the discretized fluid modeling equation are

$$\frac{\phi_{i+1}^{t+\Delta t} - 2\phi_i^{t+\Delta t} + \phi_{i-1}^{t+\Delta t}}{(\Delta x)^2} = -\frac{1}{\epsilon_0} \left( \sum_{i=1}^k (\text{sign}) n_i - n_e \right)_i^{t+\Delta t}$$

$$\frac{n_{p,e,uc}^{t+\Delta t} - n_{p,e,uc}^t}{\Delta t} + \frac{(\Gamma_{p,e,uc})_{i+1/2}^{t+\Delta t} - (\Gamma_{p,e,uc})_{i-1/2}^{t+\Delta t}}{\Delta x} = (S_{p,e,uc})^{t+\Delta t}$$

$$\frac{n_{\varepsilon}^{t+\Delta t} - n_{\varepsilon}^t}{\Delta t} + \frac{(\Gamma_{\varepsilon})_{i+1/2}^{t+\Delta t} - (\Gamma_{\varepsilon})_{i+1/2}^{t+\Delta t}}{\Delta x} = (S_{\varepsilon})^{t+\Delta t}$$

, the flux term of this equation are

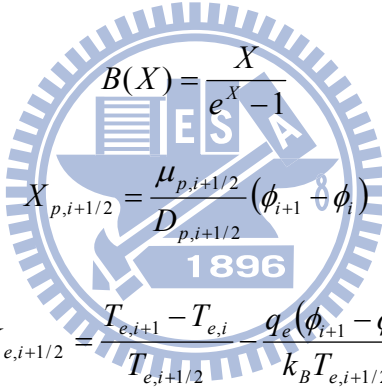
$$\Gamma_{e,i+1/2} = -\frac{1}{\Delta x} \frac{k_B T_e}{m_e v_m} [n_{e,i+1} B(-X_{e,i+1/2}) - n_{e,i} B(X_{e,i+1/2})]$$

$$\Gamma_{p,i+1/2} = -\frac{D_{p,i+1/2}}{\Delta x} [n_{p,i+1} B(-X_{p,i+1/2}) - n_{p,i} B(X_{p,i+1/2})]$$

$$\Gamma_{uc,i+1/2} = D_{p,i+1/2} \frac{n_{uc,i+1} - n_{uc,i}}{\Delta x}$$

$$\Gamma_{\varepsilon,i+1/2} = \frac{5}{2} T_{e,i+1/2} \Gamma_{e,i+1/2} - \frac{5}{2} \frac{n_{e,i+1/2} T_{e,i+1/2}}{m_e v_m} \frac{T_{e,i+1} - T_{e,i}}{\Delta x}$$

, where



$$B(X) = \frac{X}{e^X - 1}$$

$$X_{p,i+1/2} = \frac{\mu_{p,i+1/2}}{D_{p,i+1/2}} (\phi_{i+1} - \phi_i)$$

$$X_{e,i+1/2} = \frac{T_{e,i+1} - T_{e,i}}{T_{e,i+1/2}} - \frac{q_e (\phi_{i+1} - \phi_i)}{k_B T_{e,i+1/2}}$$

### 2.2.3 Parallel Fully Implicit Newton-Krylov-Swartz-Algorithm

In this thesis, the parallel fully implicit Newton-Krylov-Swartz algorithm [X. C. Cai *et al.*, 1998]<sup>[13]</sup> are used to solve the large sparse system of discretized nonlinear equations, which are derived in the previous section. Jacobian matrix is evaluated from the global vector. This scheme solves the coupled equations directly, rather than solving the equations one by one. Therefore, this fully implicit scheme allows much

larger time step and have better time accuracy than semi-implicit or explicit scheme, and has much better parallel performance when the grain size is large.

The jacobian matrix, which evaluated finite difference for Newton corrections, are solved with a preconditioned Krylov subspace type method. This Krylov method requires a preconditioning to achieve an acceptable convergence speed of inner iterations. A good preconditioner saves time and storage memory through the number of iterations in the Krylov loop and memory of the Krylov subspace are less. In this thesis, the Additive Schwarz (AS) preconditioner with the inexact solver, Newton method, in each sub-domain are used. Combining the AS preconditioner with Newton method sub-domain solver and Krylov type subspace method GMRES [Y. Saad and M. H. Schultz, 1986] for the coupled fully implicit solver: Newton-Krylov-Swartz algorithm [X. chuan Cai *et al.*, 1998]. All the preconditioner and matrix solver are employed by PETSc package [S. Balay *et al.*, 2001], which is a suite of data structures and routines for the parallel solution of the partial differential equations.

## Chapter 3 Results and Discussions

### 3.1 Simulation Conditions

A sketch of one dimensional Dielectric Barrier Discharge (DBD) with AC voltage is shown in *Figure 1* and the simulated condition is summarized in *Table 1*. The DBD with pure nitrogen gas is at atmosphere pressure, and the discharge gap is 1 mm between two dielectric barriers, which the thickness is 1 mm, the area is 25 cm<sup>2</sup> and the ceramic dielectric has permittivity 11.63. Two electrodes are connected to each dielectric barrier, and the right electrode is grounded. The left electrode is applied a 60 kHz voltage, and its waveform is measured from experiment and shown in *Figure 2*. In this simulation, the secondary electron emission or other surface reactions are not considered.

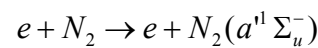
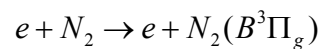
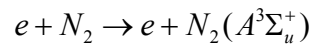
The simple chemistry reactions are summarized in *Table 2*, there are electron, 2 positive ion ( $N_2^+$ ,  $N_4^+$ ), 9 rotational and vibrational of  $N_2$  ( $N_2(rot)$ ,  $N_2(v=1-8)$ ), and 4 metastables ( $N_2(A^3\Sigma_u^+)$ ,  $N_2(B^3\Pi_g)$ ,  $N_2(C^3\Pi_u)$ ,  $N_2(a^1\Sigma_u^-)$ ). The ionization by electron impacts the rotational and vibrational state of nitrogen are not considered, that means that the rotational and vibrational species are only return to the ground state. Furthermore, the number density of background nitrogen does not change with time or position is assumed. Therefore, there are only 9 unknowns

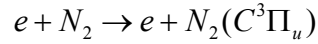
$(\phi, T_e, e, n_{N_2^+}, n_{N_4^+}, n_{N_2(A^3)}, n_{N_2(B^3)}, n_{N_2(C^3)}, n_{N_2(a^1)})$  at each grid points. The 200 uniform grids is used in the discharge gap, so the governed matrix size is about  $1800 \times 1800$ .

### 3.2 Plasma Chemistry

The nitrogen chemistry is study for the simulation of nitrogen DBD, and only 8 species,  $N_2$ ,  $N_2(A^3)$ ,  $N_2(B^3)$ ,  $N_2(C^3)$ ,  $N_2(a^1)$ ,  $N_2^+$ ,  $N_4^+$  and electron are considered. The densities of  $N^+$  and  $N_3^+$  ions are neglected at atmospheric pressure since the threshold energy of dissociative ionization is much higher than direct ionization. All the reaction channels of nitrogen chemistry are listed in *Table 2*, which including momentum transfer, rotation, vibration, ionization, excitation and recombination reactions. The sketch of reaction channels are shown in *Figure 3*, which the species are ordered as the energy levels.

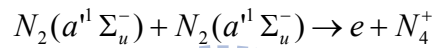
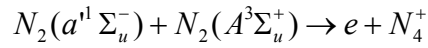
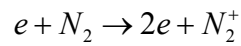
The reaction channels of momentum transfer, rotation and vibration reactions, from No.1 to No.10 listed in *Table 2*, are considered in the model for calculating the electron energy loss. The meta-stable nitrogen molecules,  $N_2(A^3)$ ,  $N_2(B^3)$ ,  $N_2(C^3)$  and  $N_2(a^1)$ , are generated since the reactions listed in No. 11, to No.14 .





These reactions are also considered for the energy loss of electron. However, the reactions channel used in this simulation do not consider ionization from excited or vibrational states.

The ionized processes considered in the chemistry model are No. 15 to No.17,

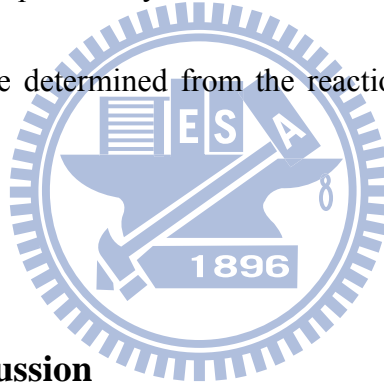


The No.15 reaction can generate electron efficiency at high electron temperature, and No.16 and No.17 are ionized process from excited state, which are the dominant process to maintain the nitrogen plasma.

The reaction rate of radiative transition between two excited or metastable states determines the intensities of the optical emissions. Since the reason, the reaction channels from No.27 to No.30 listed in *Table 2* can simulate the intensities of several optical emissions of different wavelengths, which are 177.1 nm, 293 nm, 336.5 nm and 1045 nm.

At atmospheric pressure, the electron energy distribution function (EEDF) is assumed Maxwellian distribution, and the cross sections of each reaction channels are provided from BOLSIG+. The reaction rate coefficients can be evaluated by

integrating the EEDF, and all the reaction rate coefficients which involved with electron, are shown in *Figure 4* and *Figure 5*. From *Figure 4*, it reveals that the momentum transfer reaction is the most frequency than other's reaction and the higher vibrational state of nitrogen has the lower reaction rate. *Figure 5* shows that the reaction rate coefficient of excited reactions are larger than ionized reaction when the electron in low energy (below 4 eV), but in high energy (above 8 eV) the rate coefficient of ionized reaction is higher than almost all excited reaction since the high energy electron has more probability to ionized than excited. Furthermore, the electron energy loss can be determined from the reaction and the threshold energy listed in *Table 2*.



### **3.3 Results and Discussion**

#### **3.3.1 Conduction, Displacement and Total Currents**

The total current versus with time is shown in *Figure 6*, and the total current from simulation is match able with experiment data qualitatively and quantitatively. The figure shows that the total current increases as the increasing voltage and decreases as decreasing voltage.

The total current is the sum of displacement current and conduction current of charged species.



$$J_{total} = J_{displacement} + \sum \pm e\Gamma_{e, N_2^+, N_4^+}$$

Therefore, the total can be separate into conduction currents and displacement current shown from *Figure 8 a* to *Figure 8 h*. The sketches observe that the variance of displacement and conduction currents during one cycle. In *Figure 8 a*, the applied voltage approaches to zero at initial, and the total current equals to the displacement current. As the voltage increasing at left electrode, the electron moves toward the left dielectric barrier since the high potential, so the positive conduction current of electron is generated.

On the other hand, the positive conduction currents of ions are produced due to the ions move toward right dielectric at low potential. In *Figure 8 b*, the maximum value of electron conduction current are higher than ion conduction current, because of the electron is easy to move during electric field since the mass of electron is lighter than ions,  $N_2^+$  and  $N_4^+$ .

After most electron hits the left dielectric barrier, the positive ions are moving toward the right dielectric barrier as shown in *Figure 8 c*. And then, the conduction currents approach to zero since the shielding by the accumulated surface charge.

From *Figure 8 a* to *Figure 8 h*, it also verifies that the gradient of total current equals to zero at all time,

$$\nabla \cdot J_{total} = 0$$

### 3.3.2 Power Absorptions and Light Emissions

The plasma frequency [M. A. Lieberman and A. J. Lichtenberg, 2005] of charged species  $i$  is

$$\omega_i = \sqrt{n_i e^2 / \epsilon_0 m_i}$$

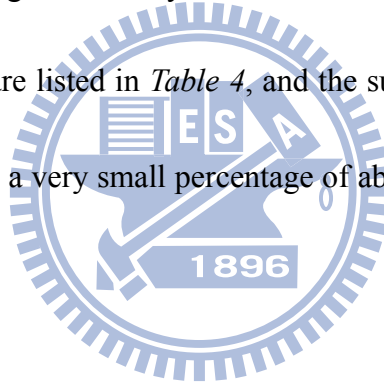
Assume  $n_e \approx 10^{16}$ ,  $n_{N_2^+} \approx 10^{17}$  and  $n_{N_4^+} \approx 5 \times 10^{16}$  which are taken from simulated results, so the plasma frequencies can be estimated as 5.6 GHz, 78.8 MHz and 39.4 MHz for electron,  $N_2^+$  and  $N_4^+$ . Since the frequency of applied voltage is 60 kHz, we expect that the both electron and ions can correspond to the driving frequency and also absorb energy from the electric field.

The absorbed power of charged species versus with time in one cycle is shows in *Figure 9*, and it shows that charged species get energy efficiently while in the stronger electric field caused by raising and falling of the applied voltage. During the time of applied voltage varies quickly, starts from 0.5  $\mu s$  to 2.5  $\mu s$  and 8.5  $\mu s$  to 11  $\mu s$ , the  $N_2^+$  absorb the most energy since the largest number density, and the other energy are absorbed by electron since the electron can respond the electric field quickly.

We take the average over one cycle to calculate the time averaged absorption power of each species listed in *Table 3*, the power absorbed by electron is 63.5 (J/s), the power absorbed by  $N_2^+$  is 267.2 (J/s), and the power absorbed by  $N_4^+$  is 2.8 (J/s).

We take time average to the absorbed power of displacement current  $(J_{dis} \cdot \vec{E})$  during one cycle, the answer is zero. It reveals that the energy which absorbed by dielectric barrier will be released during the cycle, and there is no net energy absorbed by dielectric barrier. Therefore, the total absorption power is the sum of each species, 333.6(J/s). The result shows that most energy (about 81%) is absorbed by ions and the electron absorbs the other (about 19%).

In *Figure 10*, the power of the emitted light is shown, and the emitted light of wavelength 336.5 nm has higher intensity than others' wavelength. The time averaged powers of light emissions are listed in *Table 4*, and the sum of all powers is less than 0.3%. That means that only a very small percentage of absorbed power is used for the light emissions.



### **3.3.3 Potential, Electron Temperature and Accumulated Charge**

The voltages between the dielectric barriers and the discharge gap versus with time are shown in *Figure 7*. At initial, the electron moves toward the left dielectric which carried positive charge as increasing voltage, so the negative charged is accumulated on left barrier. Although the accumulated charge approach to stable at about 2  $\mu s$ , there still has large potential gradient in the gap. Because of there is no quasi-neutral region in discharge, and the potential is not shielded by the accumulated

charge at dielectric barrier. And the gap voltage approaches to zero at about 3.5  $\mu\text{s}$  while the amplitude of applied voltage becomes small.

According to the boundary condition at left dielectric surface,

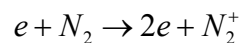
$$\epsilon_0 \frac{\partial \phi}{\partial x} - \epsilon_d \frac{\partial \phi_d}{\partial x} = -\sigma_s$$

, the distribution of potential is effected by the accumulated charge, and *Figure 7* reveal that the maximum value of accumulated charge is about 1  $\text{C}/\text{cm}^2$ . The phase diagrams of potential and electron temperature are shown in *Figure 11* and *Figure 12*.

Since the electron gets energy from the gradient of potential, the two figures show that the electron temperature is increased form 1~2  $\text{eV}$  to 4~5  $\text{eV}$  during the increasing and decreasing applied voltage. Therefore, the excited species and ions can be produced efficiently while the electron temperature approaches to 5  $\text{eV}$ .

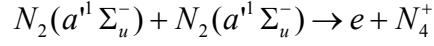
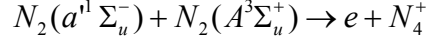
### 3.3.4 Charged Species

The number density of electron increases from  $10^{13}$  ( $1/\text{m}^3$ ) to  $10^{16}$  ( $1/\text{m}^3$ ) during the raising voltage, which shown in *Figure 13*, because the ionized process has large reaction rate coefficient at high electron temperature,



The phase diagrams of ions species  $N_2^+$  and  $N_4^+$  are shown in *Figure 14* and *Figure 15*, and it show that the increasing of  $N_2^+$  number density is depended on the

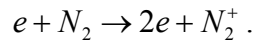
electron temperature because of the direct ionized process of nitrogen is sensitively to electron temperature. Since the associative ionized processes,



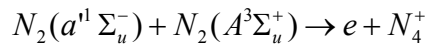
This is revealed on the phase diagrams of  $N_2(A^3)$  and  $N_2(a^1)$  number density, *Figure 16* and *Figure 17*, and the figures show that the  $N_4^+$  increases when the decreasing number density of  $N_2(A^3)$  and  $N_2(a^1)$ .

The  $N_4^+$  ion can be generated from  $N_2(A^3)$  and  $N_2(a^1)$ , so the  $N_4^+$  can still be produced efficiently during low electron temperature. Therefore, the number density of  $N_2^+$  is higher than  $N_4^+$  during the pulse of voltage, and  $N_4^+$  becomes dominated when the voltage is slightly changing.

From the electron generated or destroyed from each reaction channels, the *Figure 20* shows that the dominant process to generate electron at high electron temperature (above 3 eV) is direct ionization,



At low electron temperature (below 2 eV), during the cycle, the most electron is produced by,



The profiles of charged species versus with position are shown in *Figure 21* at 5

different time points, from *Figure 21 a* to *Figure 21 e*. The number density of electron is less than the positive ions, so there is no quasi neutral region, which is called Townsend-like discharge.

### 3.3.5 Neutral Species

The phase diagrams of neutral species are shown from *Figure 16* to *Figure 19*, and the number densities of excited species,  $N_2(A^3)$ ,  $N_2(a'^1)$ ,  $N_2(C^3)$  and  $N_2(C^3)$  which sort by the value of number density, are about  $10^{20}$ ,  $10^{18}$ ,  $10^{17}$  and  $10^{16}$ . According to simulation, the order does not change during all temporal and spatial space.

As previous discussion, the dominant reaction channels to generate electron at low electron temperature is,



Since the number densities of  $N_2(A^3)$  and  $N_2(a'^1)$  are changing slightly during one cycle as shown from *Figure 21 a* to *Figure 21 e*, so the  $N_4^+$  is produced stably through associative ionization.

### 3.3.6 Influence of Different Dielectric Permittivity

The simulated condition is the same as previous simulation except the different dielectric permittivity. The total current versus with time at different dielectric

permittivity, which is changed from 9 to 12, is shown in *Figure 22*, and it shows that the total current increases as the dielectric permittivity increasing. Since the total current is the sum of conduction currents and displacement current, the total current is increased due to the increasing conduction current during the time  $0.5 \mu s$  to  $2.5 \mu s$  and  $8.5 \mu s$  to  $11 \mu s$ . At the other time, the displacement current is the dominant component of total current.

The boundary condition at left dielectric surface is,

$$\varepsilon_0 \frac{\partial \phi}{\partial x} - \varepsilon_d \frac{\partial \phi_d}{\partial x} = -\sigma_s$$

, the profile of dielectric permittivity  $\varepsilon_d$  and accumulated charge  $\sigma_s$  is shown in *Figure 23*. From the figure, it reveal that the accumulated surface charge decreasing while the decreasing the dielectric permittivity.

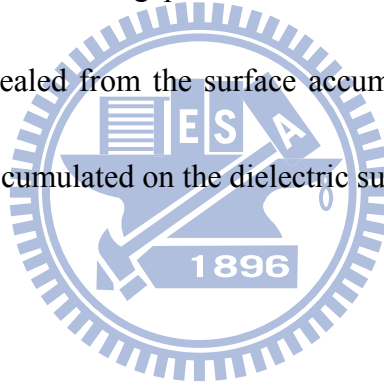
### 3.3.7 Influence of Different Gap Size

The simulated condition is the same as previous simulation, dielectric thickness 1mm with permittivity 11.63 and 60 kHz applied voltage, except that the gap size is changed. The 200 uniform grids are used for discharge gap. The total currents versus with time at different gap size, 0.5 mm, 1 mm and 2 mm, are shown *Figure 24*.

Compare the total current at different gap size, 0.5 mm and 1 mm, it shows that total current at gap size 0.5 mm is phase lead to the current at the gap size 1 mm. The

thin gap size has larger electric field than the other while applied the same waveform of voltage. While the gap size increases to 2 mm, the plasma is not maintained at this gap size, so there is no conduction current and all the total current is due to displacement current.

The accumulated charge on left dielectric surface with different gap sizes is shown in *Figure 25*. The surface charge accumulated at 0.5 mm is phase lead to 1 mm since the electron is generated earlier than the 1 mm gap, and the more electron and ions attach to the dielectric barrier at gap size 0.5 mm. The plasma does not maintain at 2 mm, and it is also revealed from the surface accumulated charge in *Figure 25*, there is almost no charge accumulated on the dielectric surface.





## Chapter 4 Conclusions and Recommendation of Future Work

### 4.1 Conclusion Remarks

The fluid modeling simulation of dielectric barrier discharge (DBD) with pure nitrogen gas is presented. The transport coefficients of nitrogen plasma and chemical reaction rate are obtained from BOLSIG, which is a Boltzmann solver can evaluate electron energy distribution function by the user given cross sections. All the model equations, species continuity equations, electron energy equation and Poisson's equation, are non-dimensionalized and discretized by fully-implicit backward Euler finite-difference method with Scharfetter-Gummel scheme for calculating the flux of charged species. The nonlinear coupled equations are solved by Newton-Krylov-Swartz (NKS) algorithm with additive Schwarz (AS) preconditioner.

The result of dielectric barrier nitrogen plasma at atmospheric pressure is presented, and the total current, which is compared with experiment data and numerical result, is acceptable. The powers of absorption and light emitted are evaluated from simulation, and it shows that the most power is absorbed by ions and the only 0.3 percentage of absorption power is cost to generate the emission of light. From the number densities of electron and positive ions, it shows that this simulation is Townsend-like discharge.

At the simulation condition which the gap size 1 mm and dielectric thickness 1

mm, the total current increases as increasing permittivity from 9 to 12, because of the large potential difference is induced by surface accumulated charge . The influence of different gap size is discussed at the same condition as below, except the dielectric permittivity is 11.63 and the gap size is changed from 0.5 mm to 2 mm. The total current of 0.5 mm gap size is phase lead to the other gap sizes due to the surface accumulated charge is the largest. Furthermore, at gap size equals 1.5 mm, the transit from Townsend-like discharge to glow discharge is observed during the current increase.

## **4.2 Recommendation of Future Work**

According to this study, the future work is suggested as following,

1. To conduct the more complicated nitrogen plasma chemistry for the light emitted on other wavelength.
2. To consider the oxygen chemistry in simulation, in order to model the dielectric barrier discharge with the mixture of nitrogen and oxygen.

## Reference

- [1] Chieh-Tsan Hung, Yuan-Ming Chiu, Feng-Nan Hwang, Jong-Shinn Wu, “Development of a Parallel Implicit Numerical Solver of 2D Fluid Modeling Equations for Gas Discharges,” *Manuscript submitted for publication*.
- [2] E. Panousis, L. Papageorghiou, N. Spyrou, J. F. Loiseau, B. Held and F. Clement, “Numerical modeling of an atmospheric pressure dielectric barrier discharge in nitrogen: electrical and kinetic description,” *J. Phys. D: Appl. Phys.*, vol. 40, pp. 4168-4180, 2007.
- [3] F. Massines, P. Segur, N. Gherardi, C. Khamphan and A. Richard, “Physics and chemistry in a glow dielectric barrier discharge at atmospheric pressure: diagnostics and modeling,” *Surface and Coatings Technol.*, pp. 8-14, 2003.
- [4] Gerjan Hagelaar, Software, “Bolsig (shareware)”, 2000.
- [5] L. Papageorghiou, E. Panousis, J. F. Loiseau, N. Spyrou and B. Held, “Two-dimensional modeling of a nitrogen dielectric barrier discharge (DBD) at atmospheric pressure: filament dynamics with the dielectric barrier on the cathode,” *J. Phys. D: Appl. Phys.*, vol. 42, 2009.
- [6] M. Capitelli, C. M. Ferreira, B. F. Gordiets and A. I. Osipov, “Plasma Kinetics in Atmospheric Gases,” Springer, 2000.
- [7] K. Software, “Bolsig (shareware)”, 2000.
- [8] P. Zhang and U. Kortshagen, “Two-dimensional numerical study of atmospheric

- pressure glows in helium with impurities,” *J. Phys. D: Appl. Phys.*, vol. 39, pp. 153-163, 2006.
- [9] R. B. Bird, W. E. Stewart, and E. N. Lightfoot, “Transport phenomena,” Wiley, New York, 1960.
- [10] R. Brandenburg, V. A. Maiorov, Y. B. Golubovskii, H. E. Wagner, J. Behnke and J. F. Behnke “Diffuse barrier discharges in nitrogen with small admixtures of oxygen: discharge mechanism and transition to the filamentary regime,” *J. Phys. D: Appl. Phys.*, vol. 38, pp. 2187-2197, 2005.
- [11] S. Balay, W. D. Gropp, L. C. McInnes, and B. F. Smith, “Petsc home page,” 2001.
- [12] V. A. Maiorov and Y. B. Golubovskii, “Modelling of atmospheric pressure dielectric barrier discharges with emphasis on stability issues,” *Plasma Sources Sci. Technol.*, vol. 16, pp. S67-S75, 2007.
- [13] X. C. Cai, M. A. Casarin, F. W. Elliott, and O. B. Widlund, “Overlapping schwarz algorithms for solving helmholtz’s equation,” in Contemporary Mathematics, pp. 391–399, *American Mathematical Society*, 1998.
- [14] X. T. Deng and M. G. Kong, “Frequency range of stable dielectric-barrier discharges in atmospheric He and N<sub>2</sub>,” *IEEE Trans. on Plasma Sci.*, vol. 32, no. 4, pp. 1709-1715, 2004.
- [15] Y. B. Golubovskii, V. A. Maiorov, J. Behnke and J. F. Behnke, “Influence of interaction between charged particles and dielectric surface over a homogeneous

barrier discharge in nitrogen,” *J. Phys. D: Appl. Phys.*, vol. 35, pp. 751-761, 2002.

[16] Y. H. Choi, J. H. Kim and Y. S. Hwang, “One-dimensional discharge simulation of nitrogen DBD atmospheric pressure plasma,” *Thin Solid Films*, pp.289-395, 2006.

[17] Y. Saad and M. H. Schultz, “Gmres: a generalized minimal residual algorithm for solving nonsymmetric linear systems,” *SIAM J. Sci. Stat. Comput.*, vol. 7, no. 3, pp. 856–869, 1986.

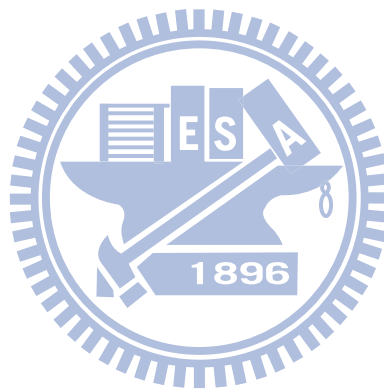


Table 1: The simulated condition of dielectric barrier discharge with pure nitrogen.

Discharge Region			Dielectric Barrier		Applied Voltage	
Gas	Pressure	Gap Size	Dielectric thickness	Permittivity	Frequency	Waveform
Pure nitrogen	760 torr	1 mm	1 mm	11.63	60 kHz	Figure 2

Table 2. Nitrogen Plasma Chemistry

No.	Reaction Channel	Threshold Energy (eV)	Rate Coefficient	
(1)	$e + N_2 \rightarrow e + N_2$	0.00	cross section	[4]
(2)	$e + N_2 \rightarrow e + N_2(\text{rot})$	0.02	cross section	[4]
(3)	$e + N_2 \rightarrow e + N_2(v=1)$	0.29	cross section	[4]
(4)	$e + N_2 \rightarrow e + N_2(v=2)$	0.59	cross section	[4]
(5)	$e + N_2 \rightarrow e + N_2(v=3)$	0.88	cross section	[4]
(6)	$e + N_2 \rightarrow e + N_2(v=4)$	1.17	cross section	[4]
(7)	$e + N_2 \rightarrow e + N_2(v=5)$	1.47	cross section	[4]
(8)	$e + N_2 \rightarrow e + N_2(v=6)$	1.76	cross section	[4]
(9)	$e + N_2 \rightarrow e + N_2(v=7)$	2.06	cross section	[4]
(10)	$e + N_2 \rightarrow e + N_2(v=8)$	2.35	cross section	[4]
(11)	$e + N_2 \rightarrow e + N_2(A^3\Sigma_u^+)$	6.17	cross section	[4]
(12)	$e + N_2 \rightarrow e + N_2(B^3\Pi_g)$	7.35	cross section	[4]
(13)	$e + N_2 \rightarrow e + N_2(a^1\Sigma_u^-)$	8.40	cross section	[4]
(14)	$e + N_2 \rightarrow e + N_2(C^3\Pi_u)$	11.03	cross section	[4]
(15)	$e + N_2 \rightarrow 2e + N_2^+$	15.58	cross section	[4]
(16)	$N_2(a^1\Sigma_u^-) + N_2(A^3\Sigma_u^+) \rightarrow e + N_4^+$	0.00	$5.0 \times 10^{-17} m^3 s^{-1}$	[15]

(17)	$N_2(a^1\Sigma_u^-) + N_2(a^1\Sigma_u^-) \rightarrow e + N_4^+$	0.00	$2.0 \times 10^{-16} m^3 s^{-1}$	[15]
(18)	$e + N_4^+ \rightarrow N_2(C^3\Pi_u) + N_2$	0.00	$2.0 \times 10^{-12} (T_g/T_e)^{0.5} m^3 s^{-1}$	[16]
(19)	$e + N_2^+ \rightarrow 2N$	0.00	$2.8 \times 10^{-13} (T_g/T_e)^{0.5} m^3 s^{-1}$	[16]
(20)	$e + N_2^+ \rightarrow N(^2D)$	0.00	$2.0 \times 10^{-13} (T_g/T_e)^{0.5} m^3 s^{-1}$	[16]
(21)	$N_2(A^3\Sigma_u^+) + N_2(A^3\Sigma_u^+) \rightarrow N_2(B^3\Pi_g) + N_2$	0.00	$7.7 \times 10^{-17} m^3 s^{-1}$	[16]
(22)	$N_2(A^3\Sigma_u^+) + N_2(A^3\Sigma_u^+) \rightarrow N_2(C^3\Pi_u) + N_2$	0.00	$3.0 \times 10^{-16} m^3 s^{-1}$	[16]
(23)	$N_2(B^3\Pi_g) + N_2 \rightarrow N_2(A^3\Sigma_u^+) + N_2$	0.00	$5.0 \times 10^{-17} m^3 s^{-1}$	[16]
(24)	$N_2(C^3\Pi_u) + N_2 \rightarrow N_2(a^1\Sigma_u^-) + N_2$	0.00	$1.0 \times 10^{-17} m^3 s^{-1}$	[16]
(25)	$N_2(a^1\Sigma_u^-) + N_2 \rightarrow N_2(B^3\Pi_g) + N_2$	0.00	$2.0 \times 10^{-19} m^3 s^{-1}$	[16]
(26)	$N_2(a^1\Sigma_u^-) + N_2 \rightarrow 2N_2$	0.00	$2.0 \times 10^{-19} m^3 s^{-1}$	[16]
(27)	$N_2(A^3\Sigma_u^+) \rightarrow N_2 + h\nu 293nm$	0.00	$0.5 s^{-1}$	[6]
(28)	$N_2(B^3\Pi_g) \rightarrow N_2(A^3\Sigma_u^+) + h\nu 1045nm$	0.00	$1.5 \times 10^5 s^{-1}$	[6]
(29)	$N_2(C^3\Pi_u) \rightarrow N_2(B^3\Pi_g) + h\nu 336.5nm$	0.00	$2.7 \times 10^7 s^{-1}$	[6]
(30)	$N_2(a^1\Sigma_u^-) \rightarrow N_2 + h\nu 177.1nm$	0.00	$1.0 \times 10^2 s^{-1}$	[6]

Table 3: The time average absorbed power of electron and ions. At the condition, the applied voltage (60 kHz), the gap size 1mm and dielectric thickness 1mm with permittivity 11.63.

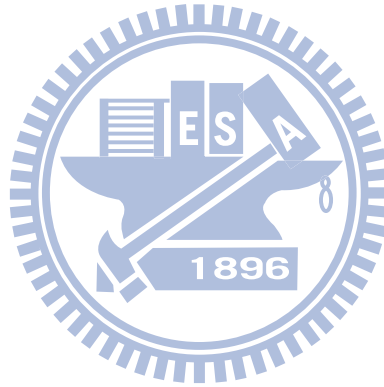
	electron	N <sub>2</sub> <sup>+</sup>	N <sub>4</sub> <sup>+</sup>	Total
Absorbed power (J/s)	63.5	267.2	2.8	333.5
Percentage	19.04 %	80.12 %	0.84 %	100 %

Total absorbed power = 333.5 (J/s)

Table 4: The time average power of light emitted. At the condition, the applied voltage (60 kHz), the gap size 1mm and dielectric thickness 1mm with permittivity 11.63.

wavelength	177.1 nm	293 nm	336.5 nm	1045 nm
Power (J/s)	1.72 x10 <sup>-4</sup>	7.8 x10 <sup>-5</sup>	0.9	4.2 x10 <sup>-4</sup>
Percentage	5.1 x10 <sup>-5</sup> (%)	2.3 x10 <sup>-5</sup> (%)	0.27 (%)	1.2 x10 <sup>-4</sup> (%)

Total absorbed power = 333.5 J/s (100%)





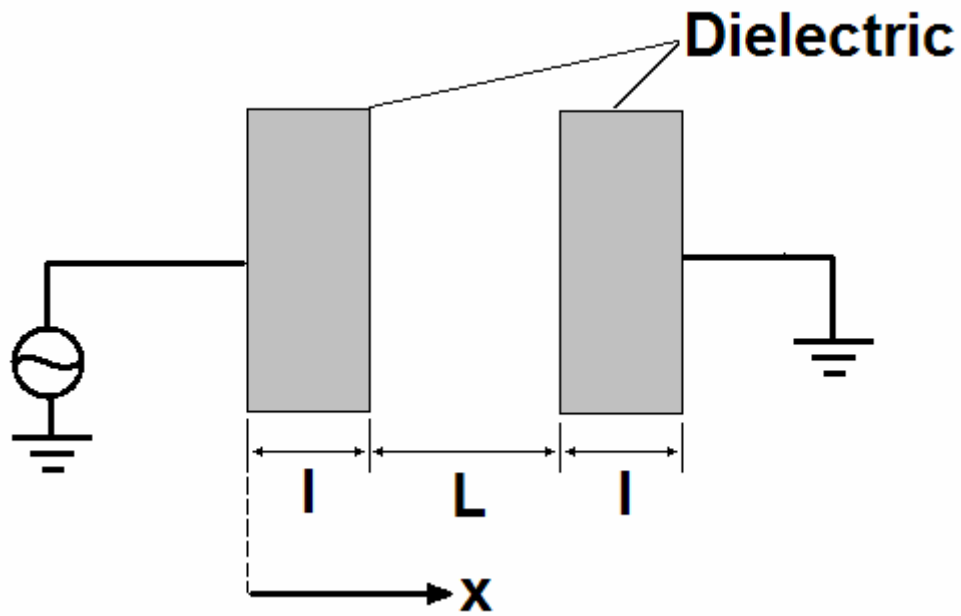


Figure 1: Sketch of 1D dielectric barrier discharge

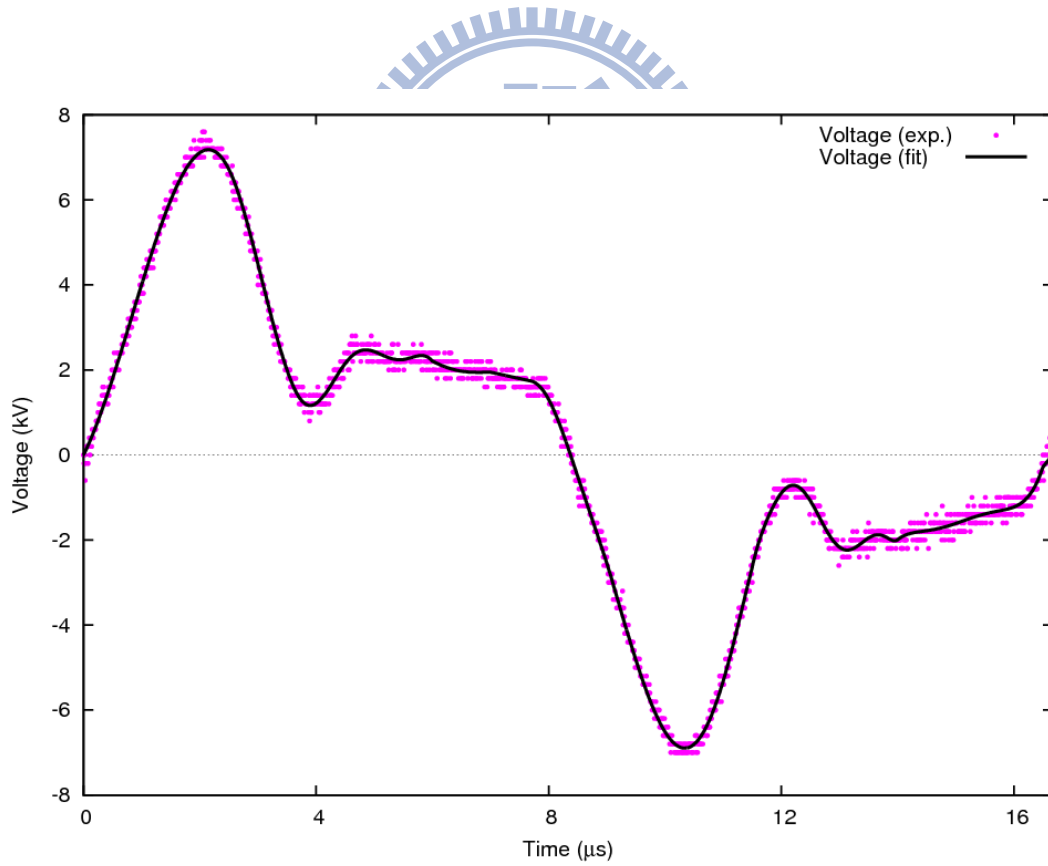


Figure 2: Waveform of the applied voltage with the frequency 60 kHz which is measured from experiment

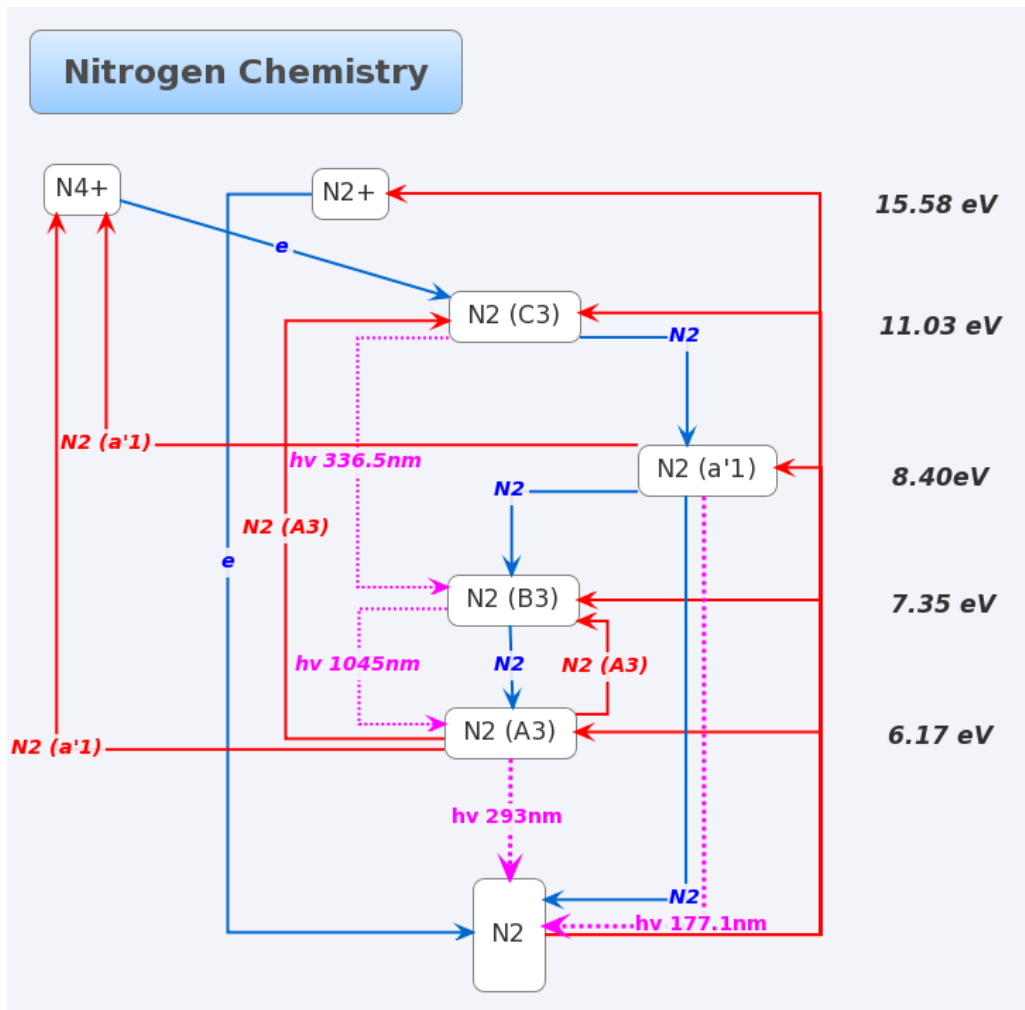


Figure 3: sketch of nitrogen plasma chemistry

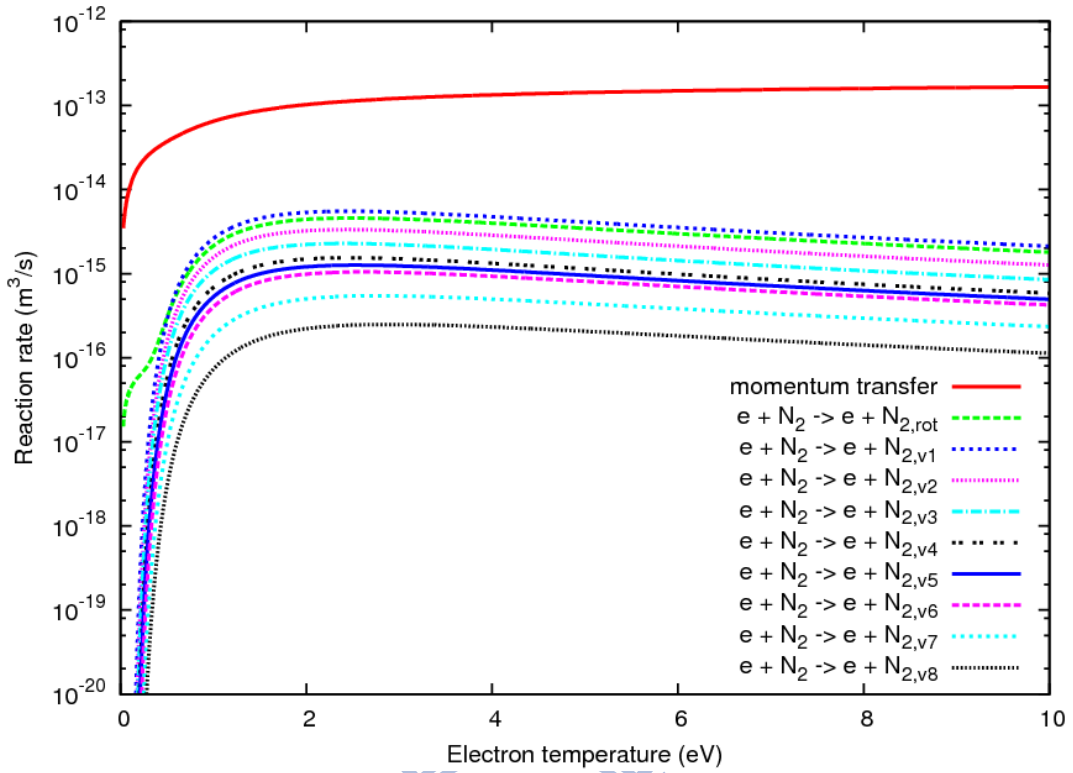


Figure 4: The reaction rate coefficients of reaction channels, from No. (1) to (10), in nitrogen plasma.

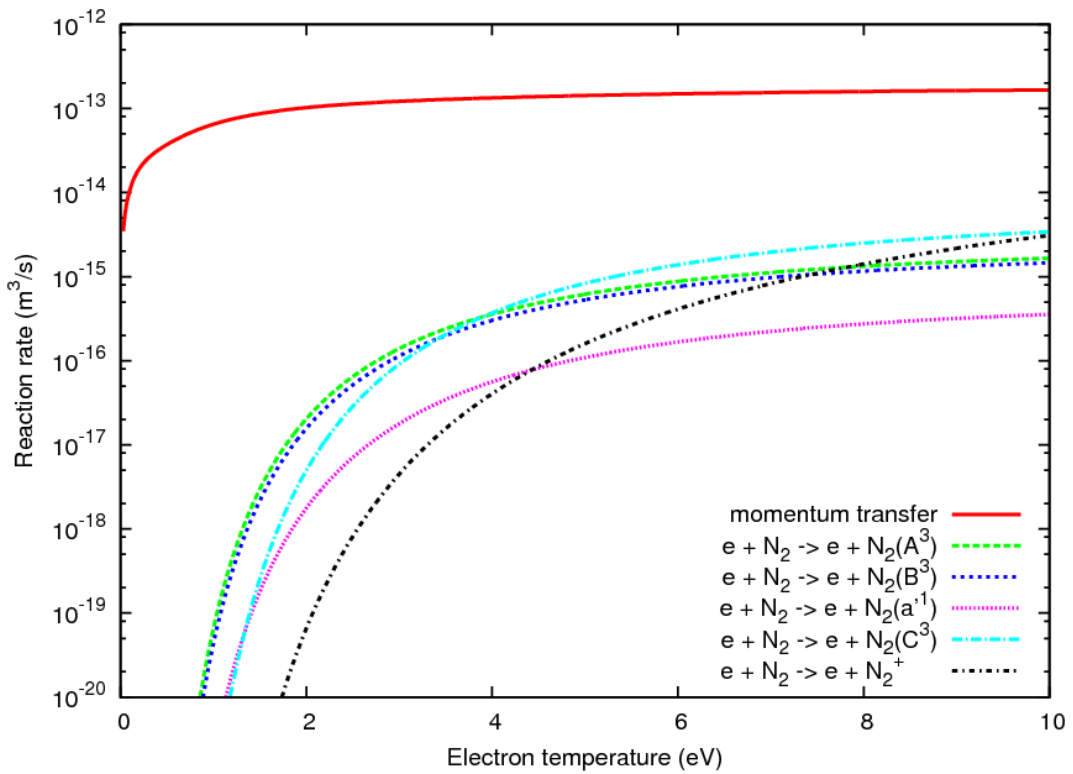


Figure 5: The reaction rate coefficients of reaction channels, from No. (11) to (15), in nitrogen plasma.

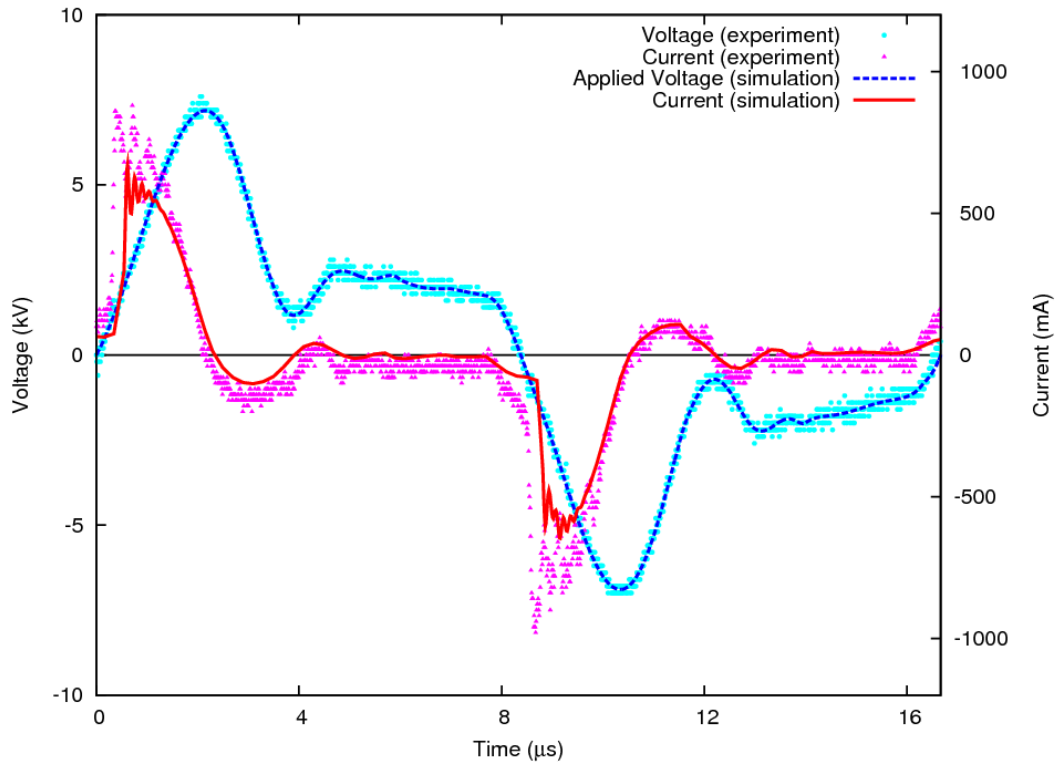


Figure 6: Total current versus with time during one cycle of applied voltage ( $60\text{ kHz}$ ) at the condition, the gap size  $1\text{ mm}$  and dielectric thickness  $1\text{ mm}$  with permittivity  $11.63$ .

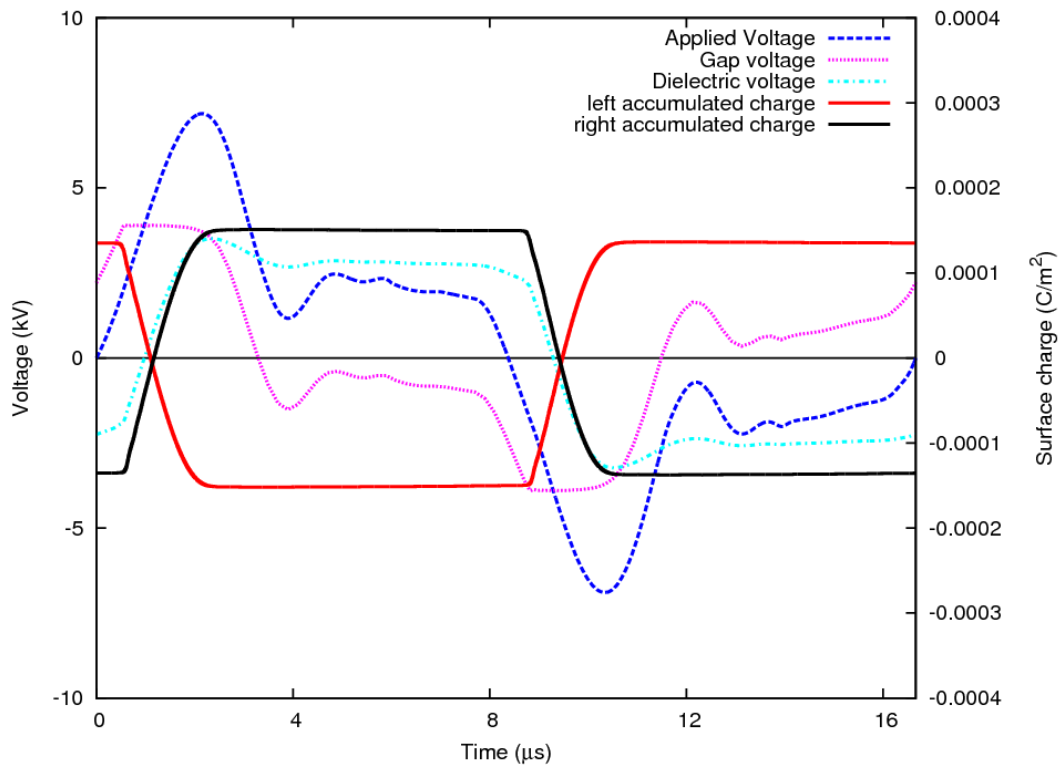


Figure 7: The gap voltage and the accumulated charge versus with time.

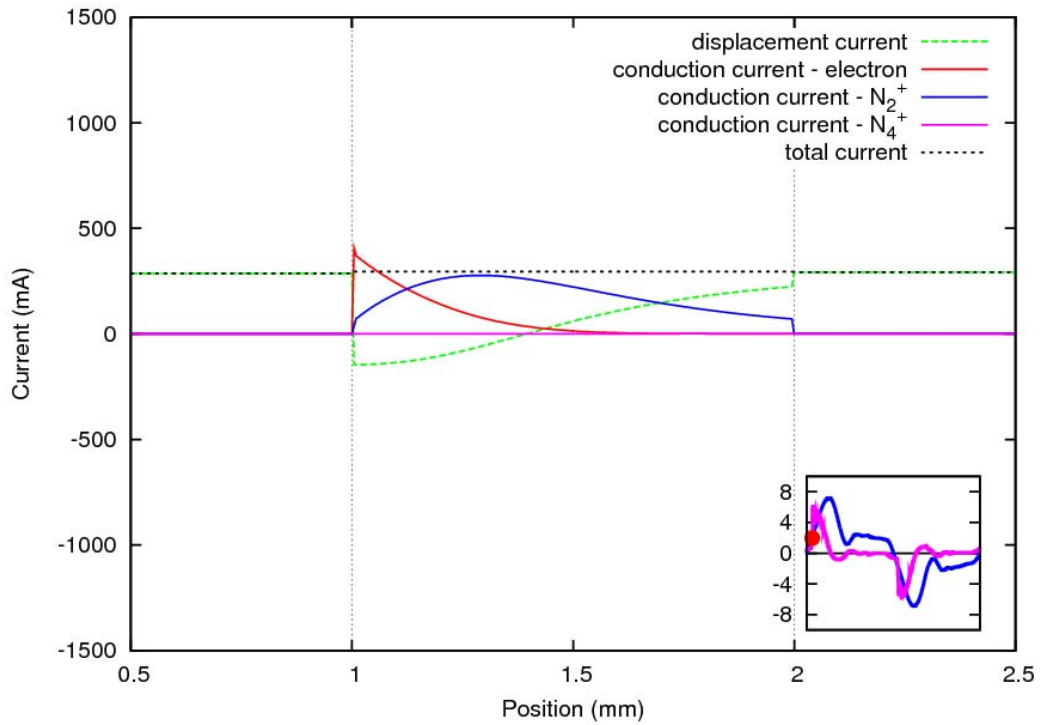
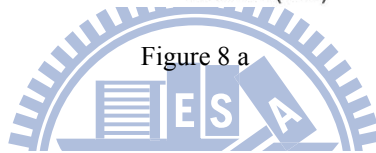
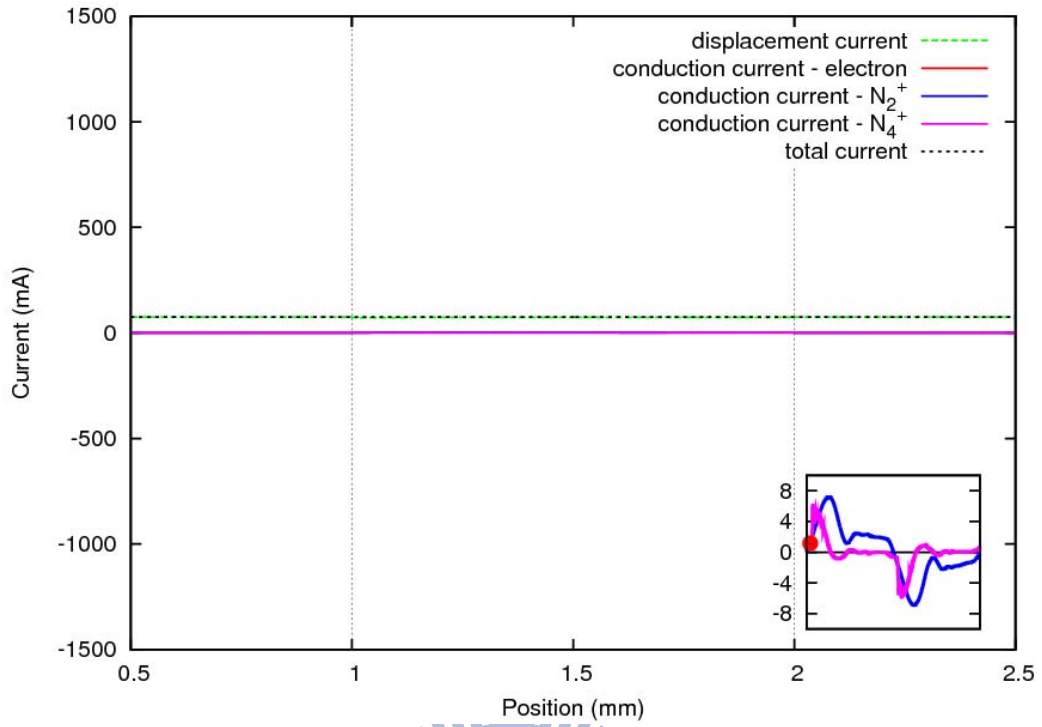


Figure 8 b

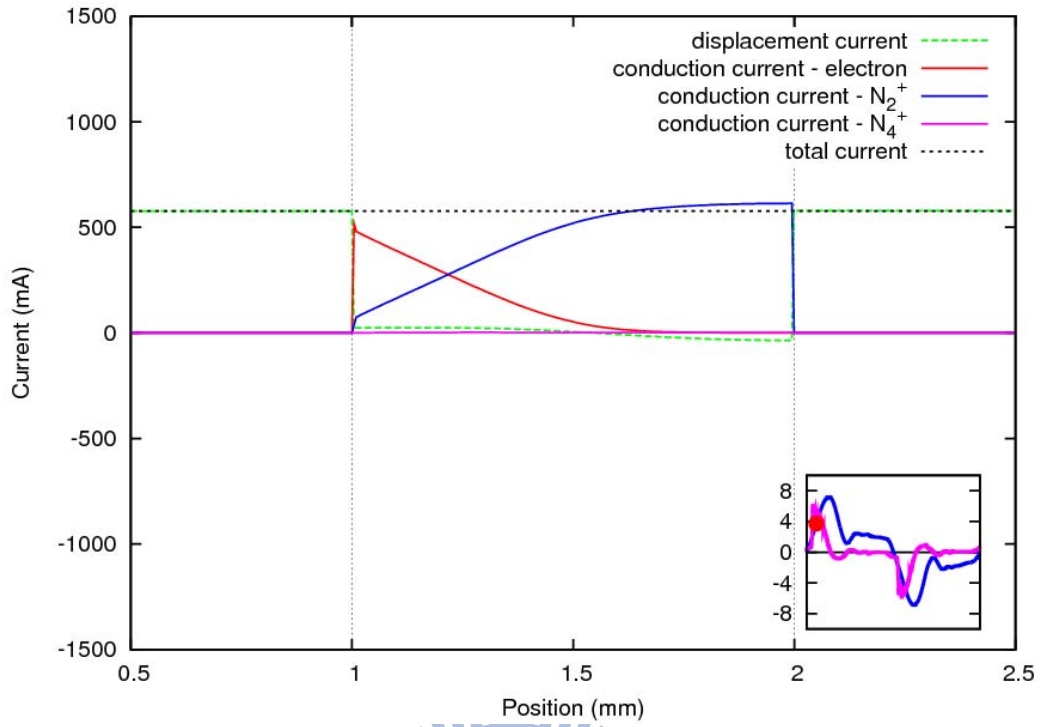


Figure 8 c

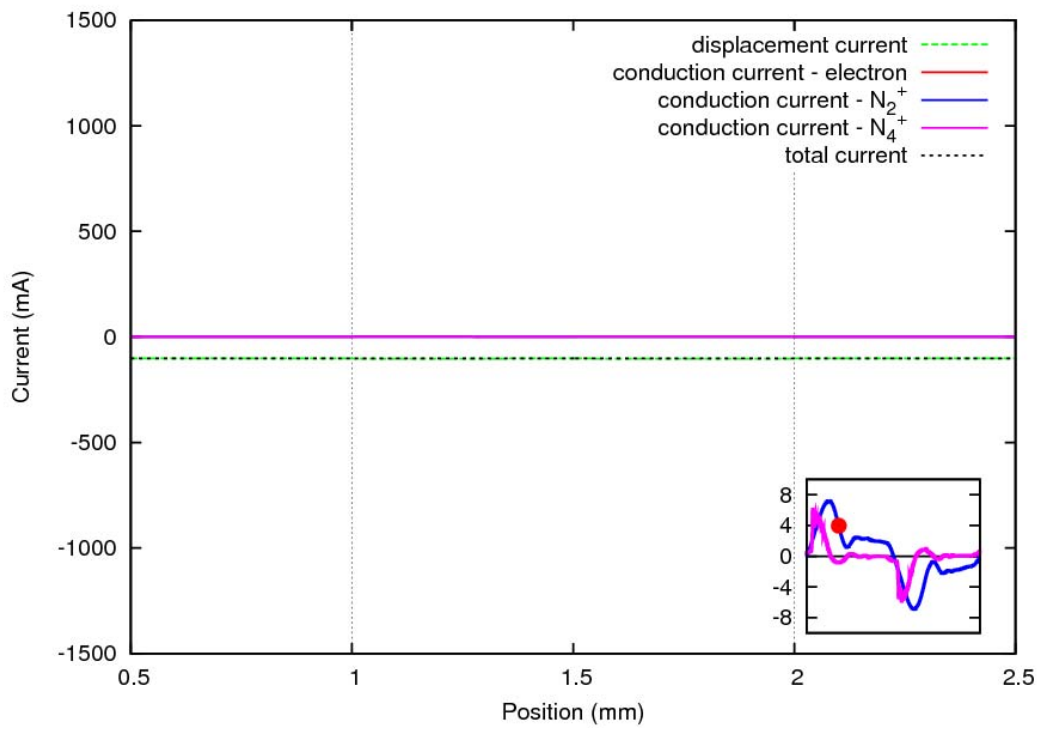


Figure 8 d

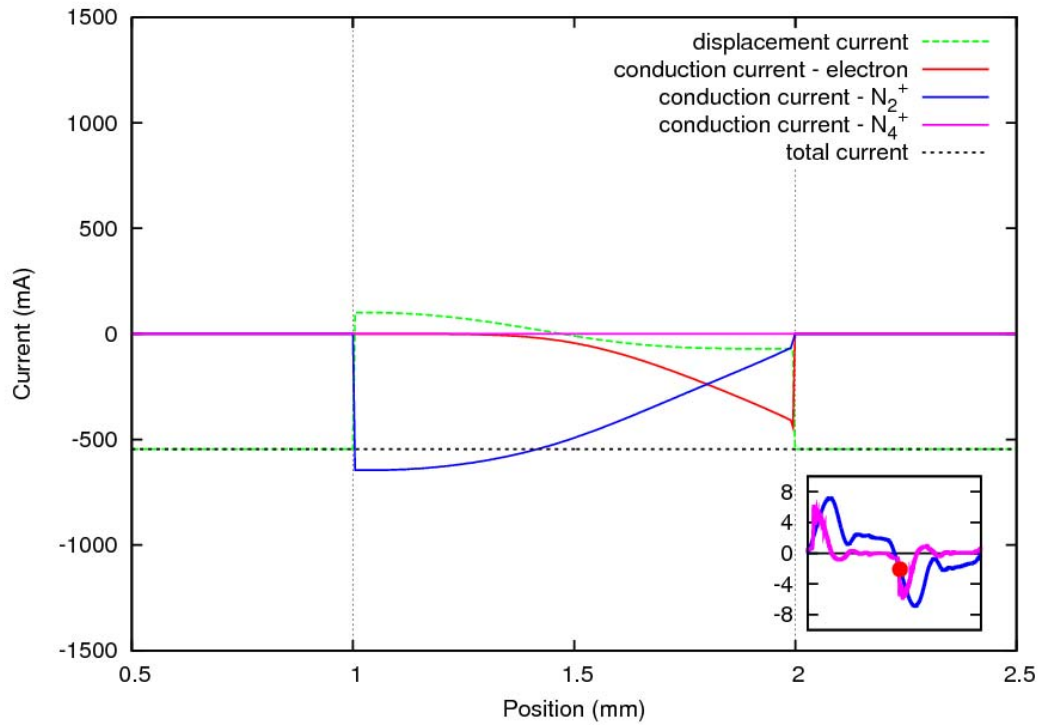
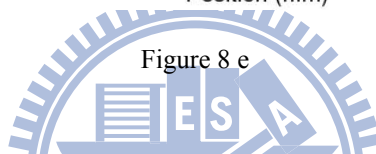
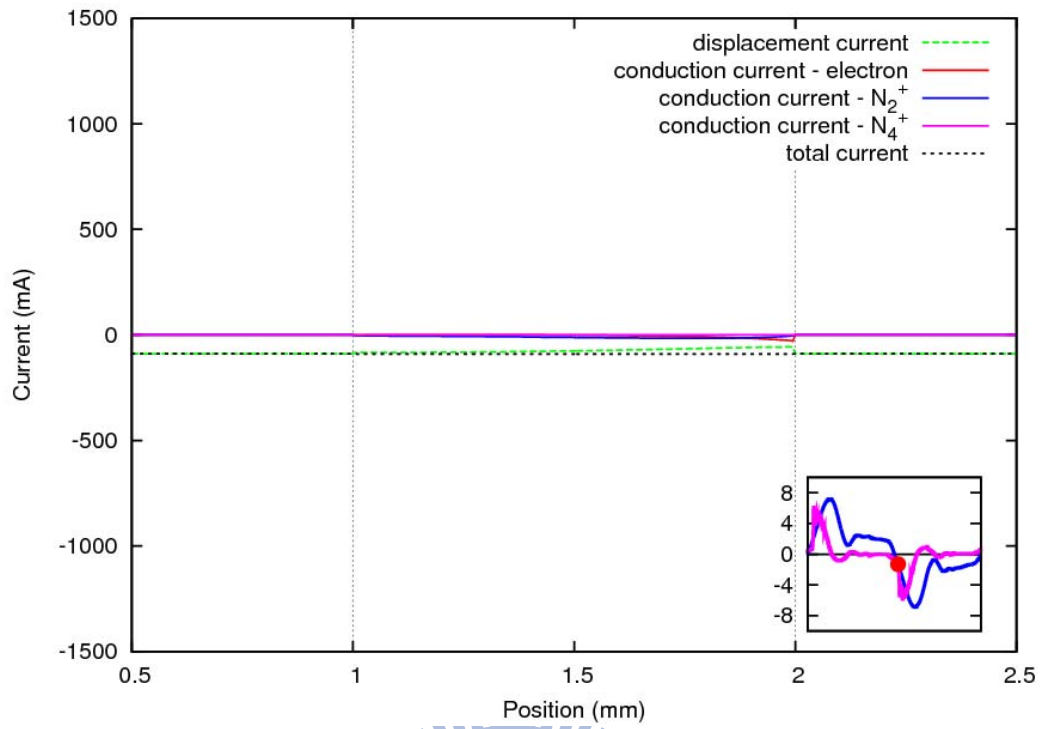


Figure 8 f

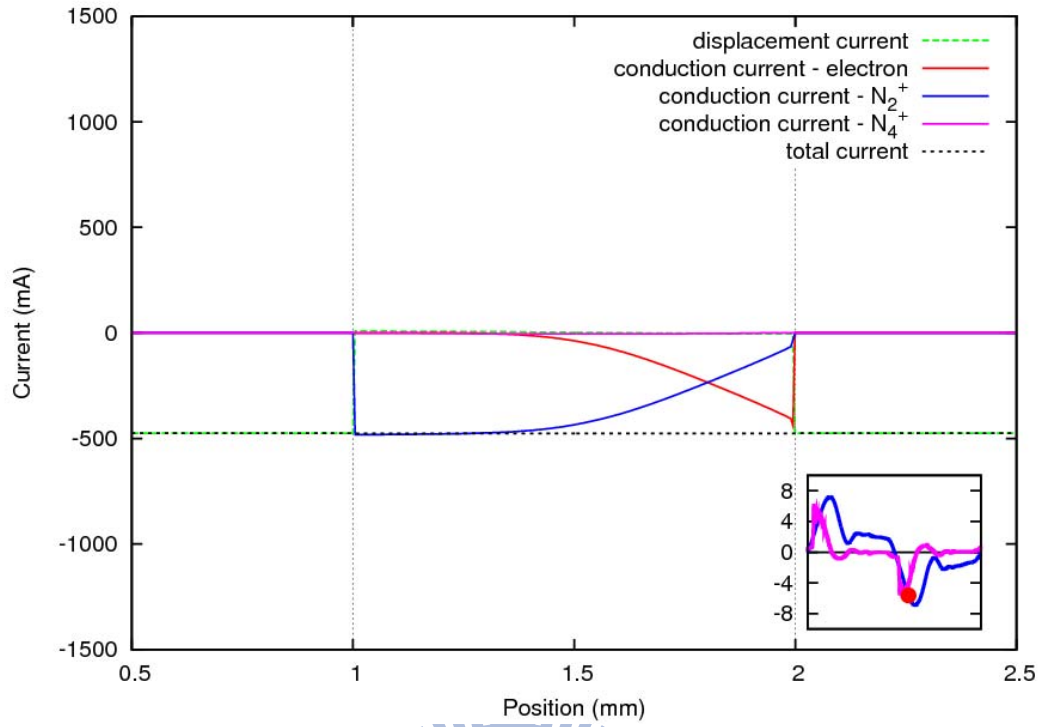


Figure 8 g

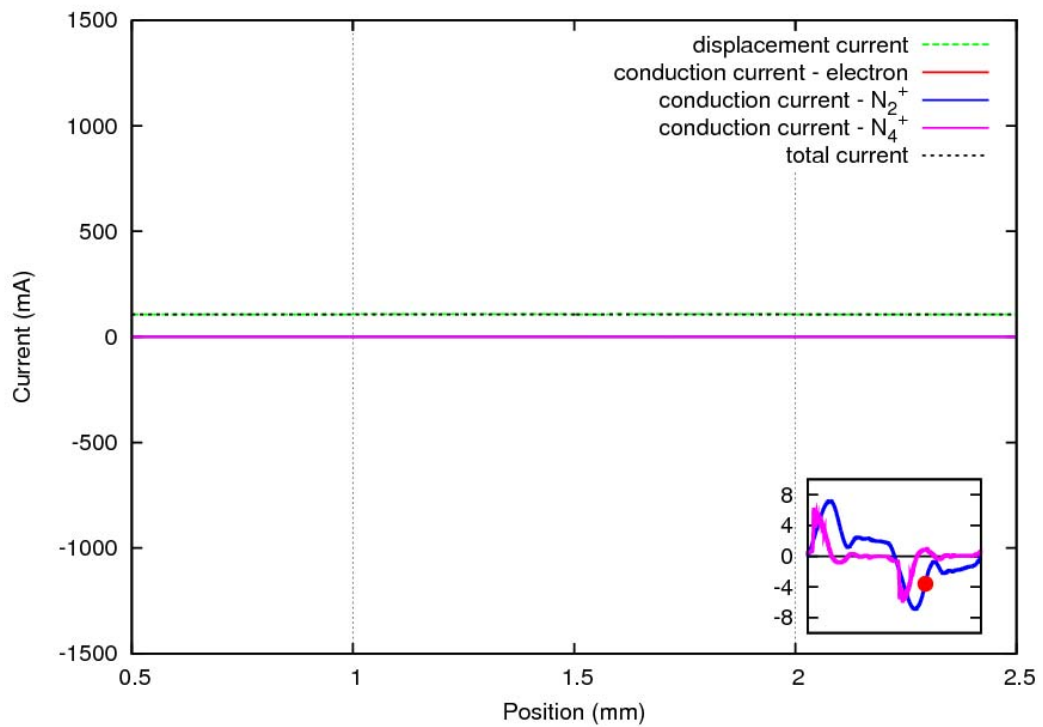


Figure 8 h

Figure 8: The displacement, conduction of charged species and the total during only cycle, *Figure 8 a* to *Figure 8 h* are shown in different time.



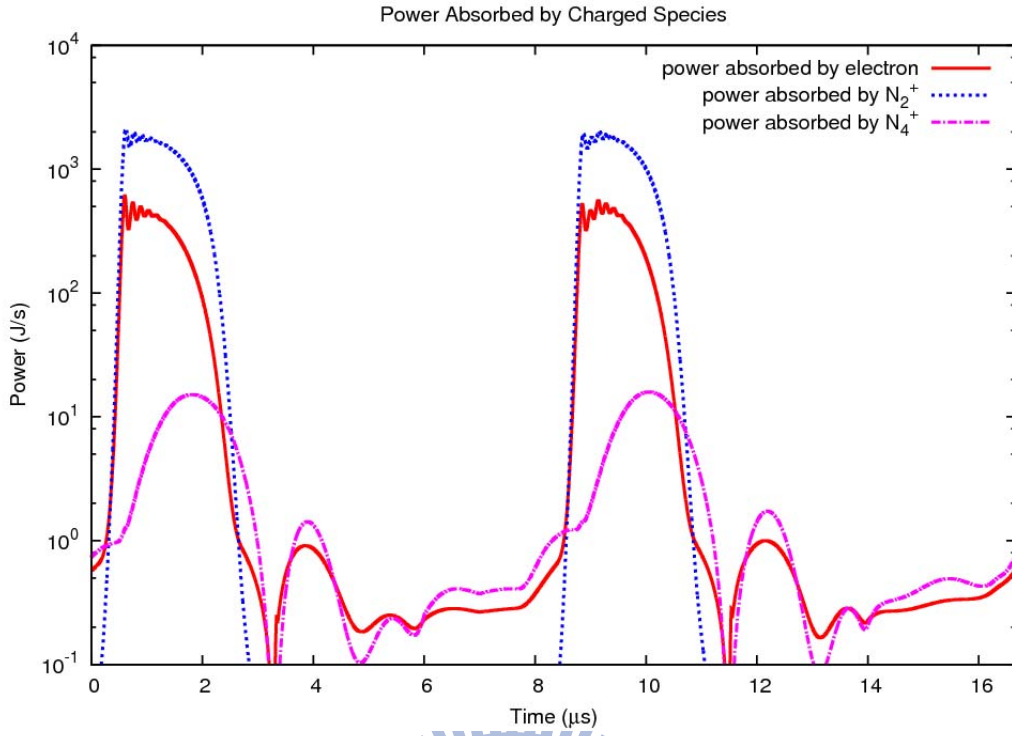


Figure 9: The power absorption of charged species at the condition, the gap size 1mm and dielectric thickness 1mm with permittivity 11.63.

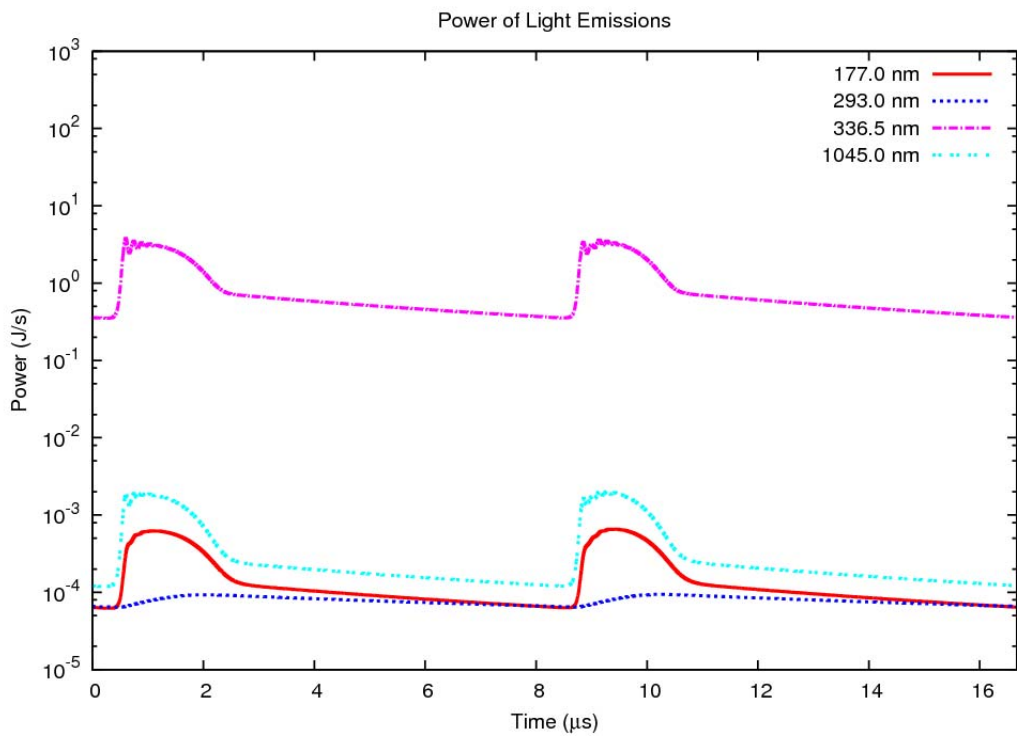


Figure 10: The power of the emitted light with different wavelength at the condition, the gap size 1mm and dielectric thickness 1mm with permittivity 11.63.

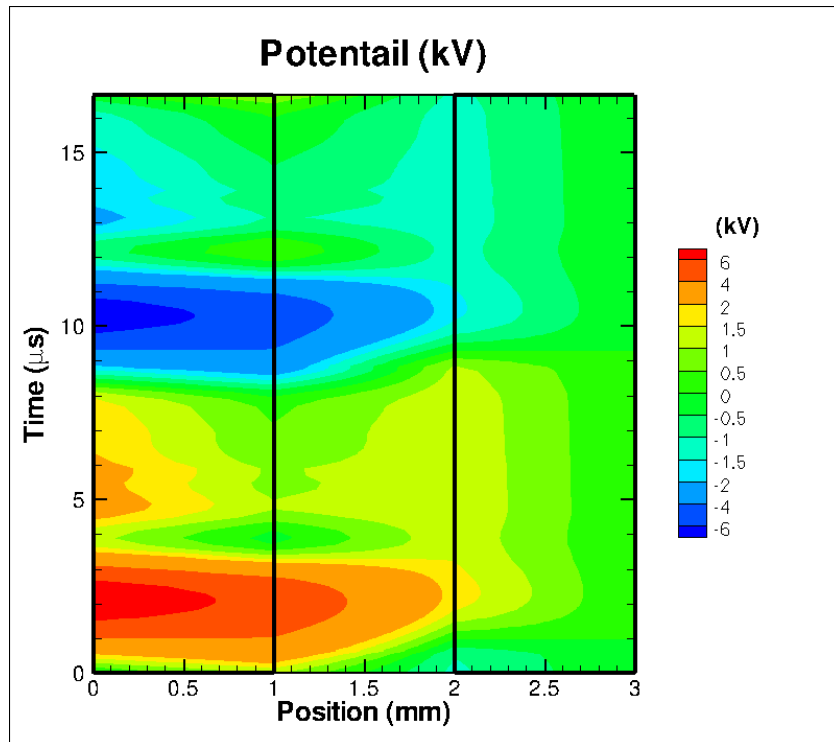


Figure 11: The phase diagram of potential with gap size 1 mm and dielectric thickness 1 mm with permittivity 11.63.

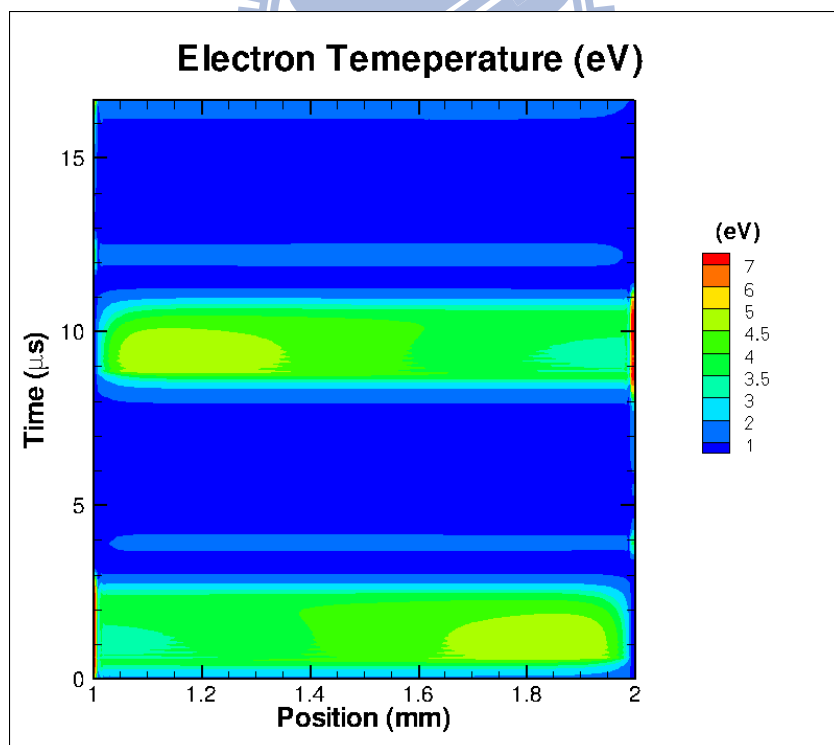


Figure 12: The phase diagram of electron temperature with gap size 1 mm and dielectric thickness 1 mm with permittivity 11.63.

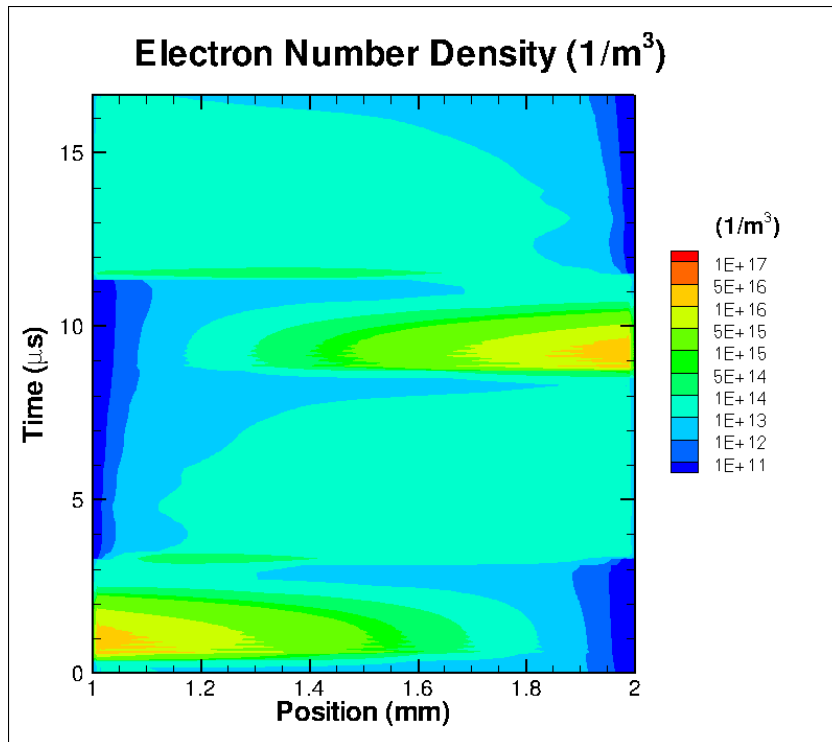


Figure 13: The phase diagram of electron number density with gap size 1 mm and dielectric thickness 1 mm with permittivity 11.63.

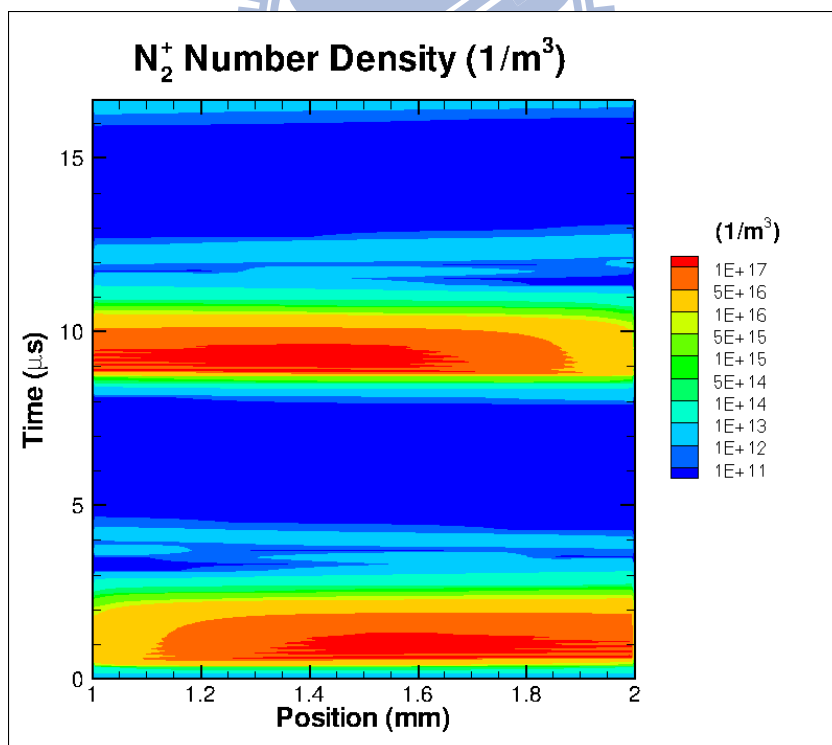


Figure 14: The phase diagram of N<sub>2</sub><sup>+</sup> number density with gap size 1 mm and dielectric thickness 1 mm with permittivity 11.63

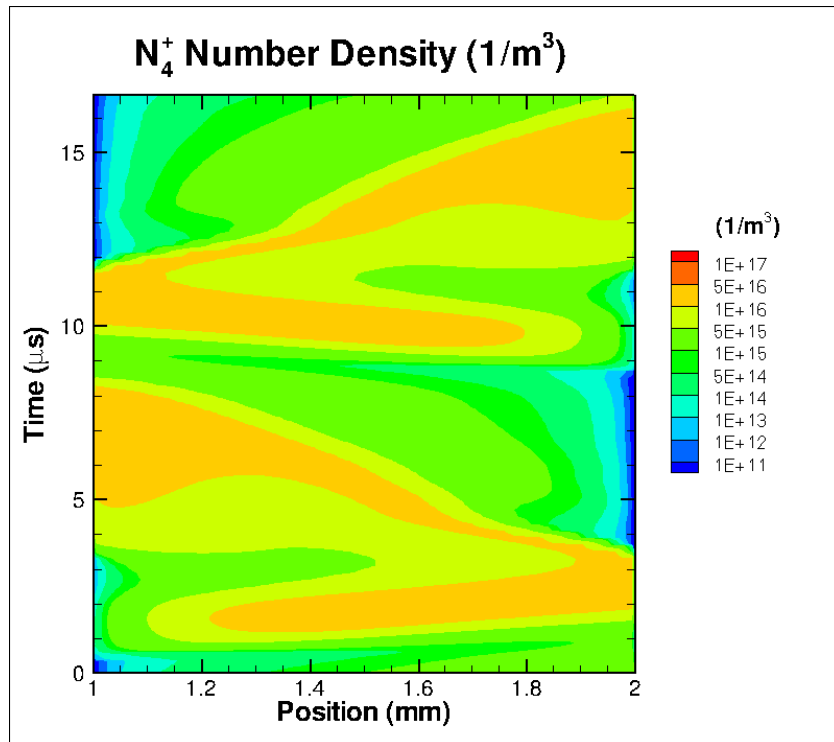


Figure 15: The phase diagram of  $N_4^+$  number density with gap size 1 mm and dielectric thickness 1 mm with permittivity 11.63

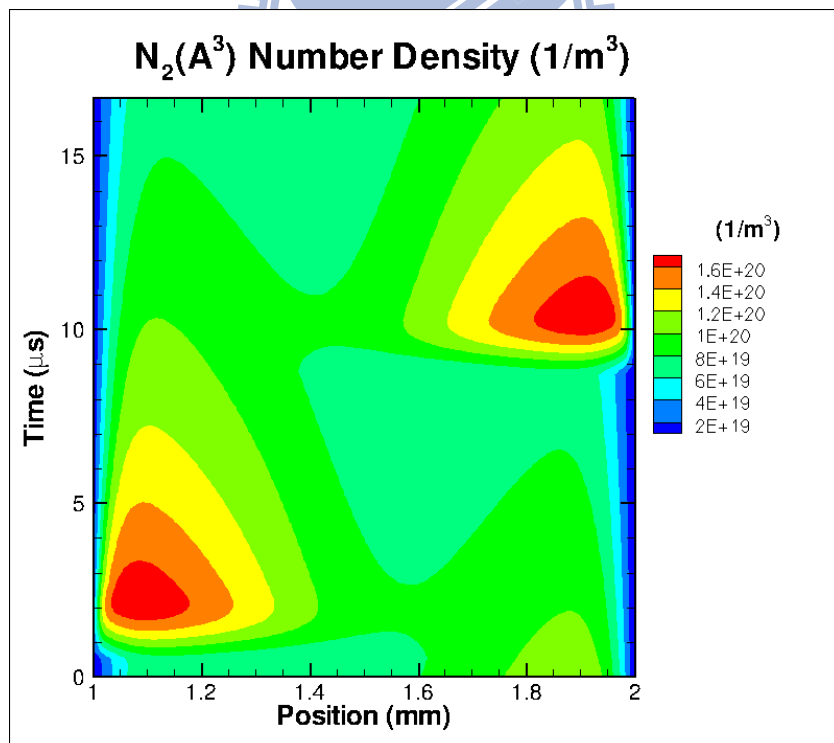


Figure 16: The phase diagram of  $N_2(A^3)$  number density with gap size 1 mm and dielectric thickness 1 mm with permittivity 11.63

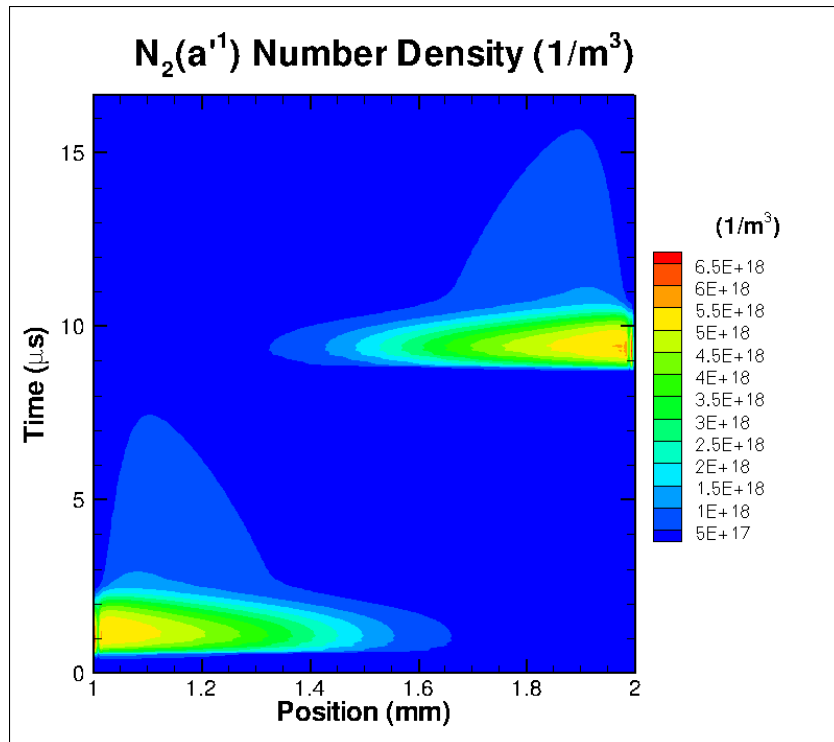


Figure 17: The phase diagram of  $N_2(a^1)$  number density with gap size 1 mm and dielectric thickness 1 mm with permittivity 11.63

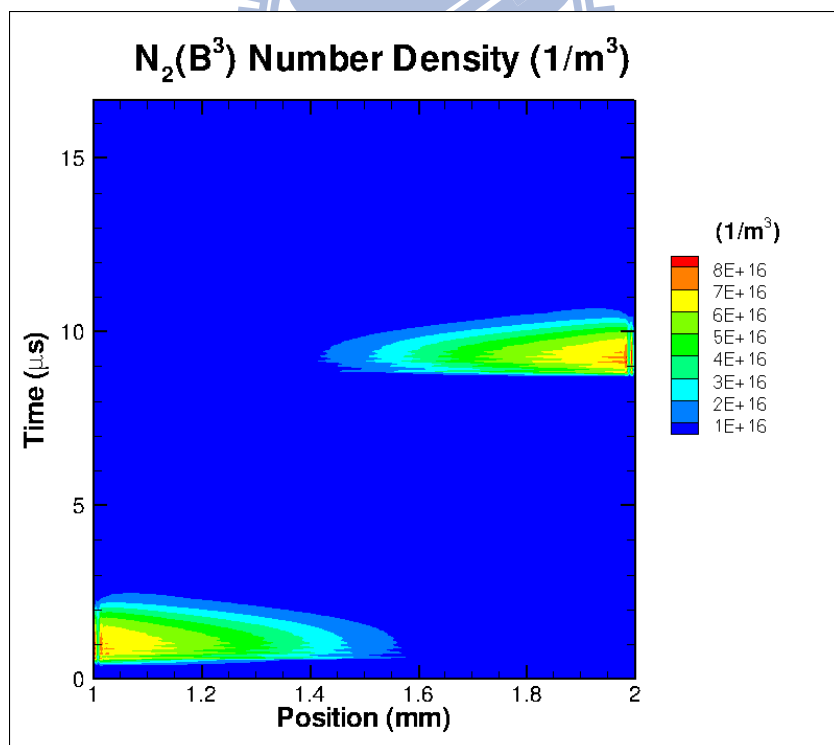


Figure 18: The phase diagram of  $N_2(B^3)$  number density with gap size 1 mm and dielectric thickness 1 mm with permittivity 11.63

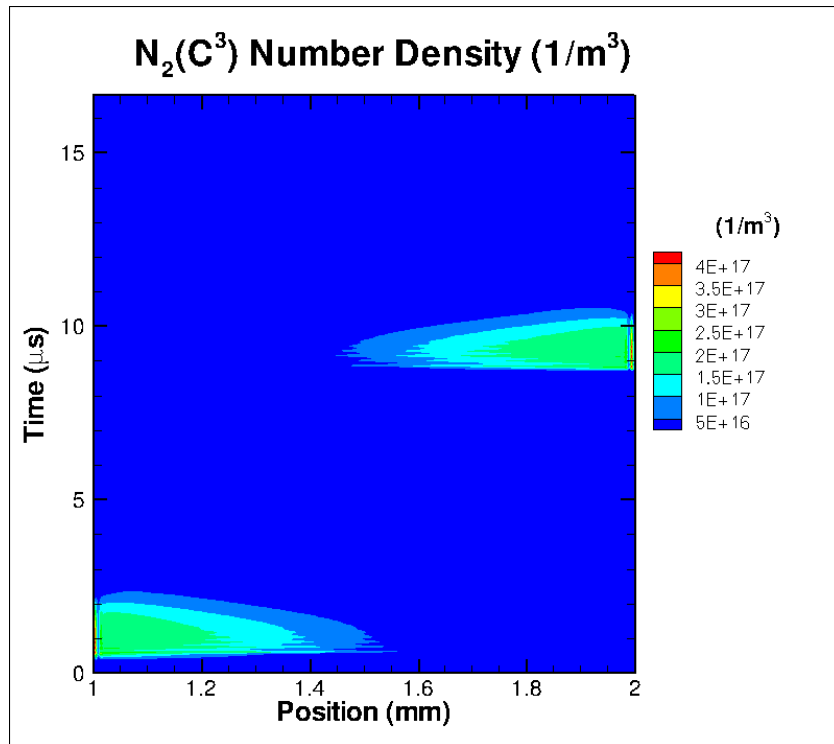
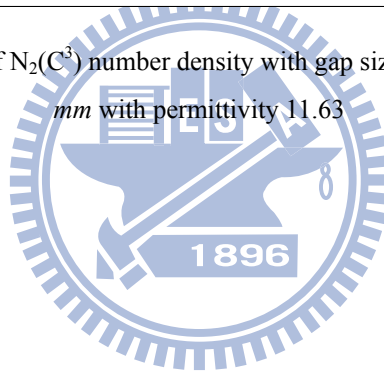
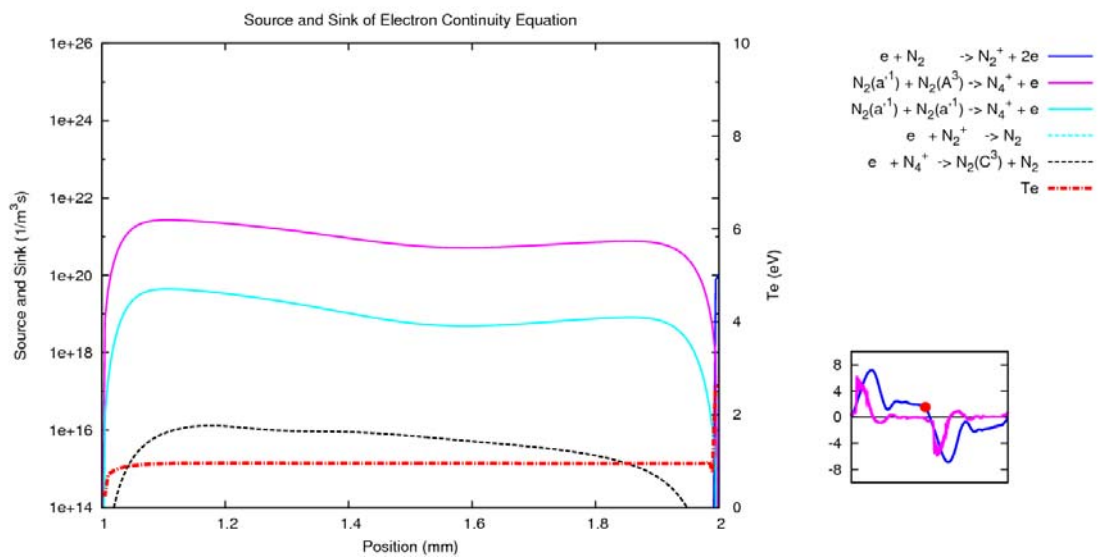
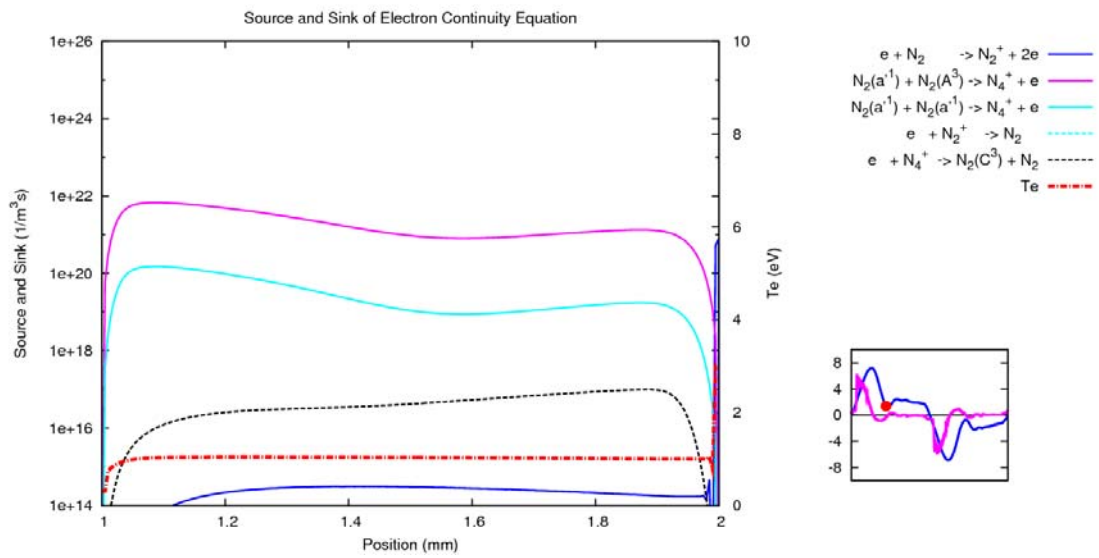
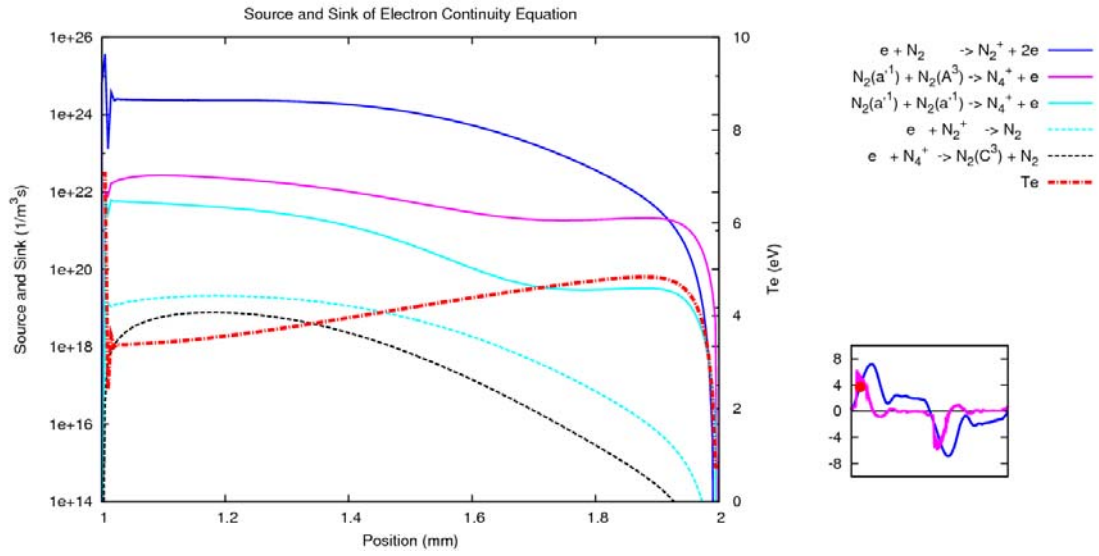


Figure 19: The phase diagram of N<sub>2</sub>(C<sup>3</sup>) number density with gap size 1 mm and dielectric thickness 1 mm with permittivity 11.63





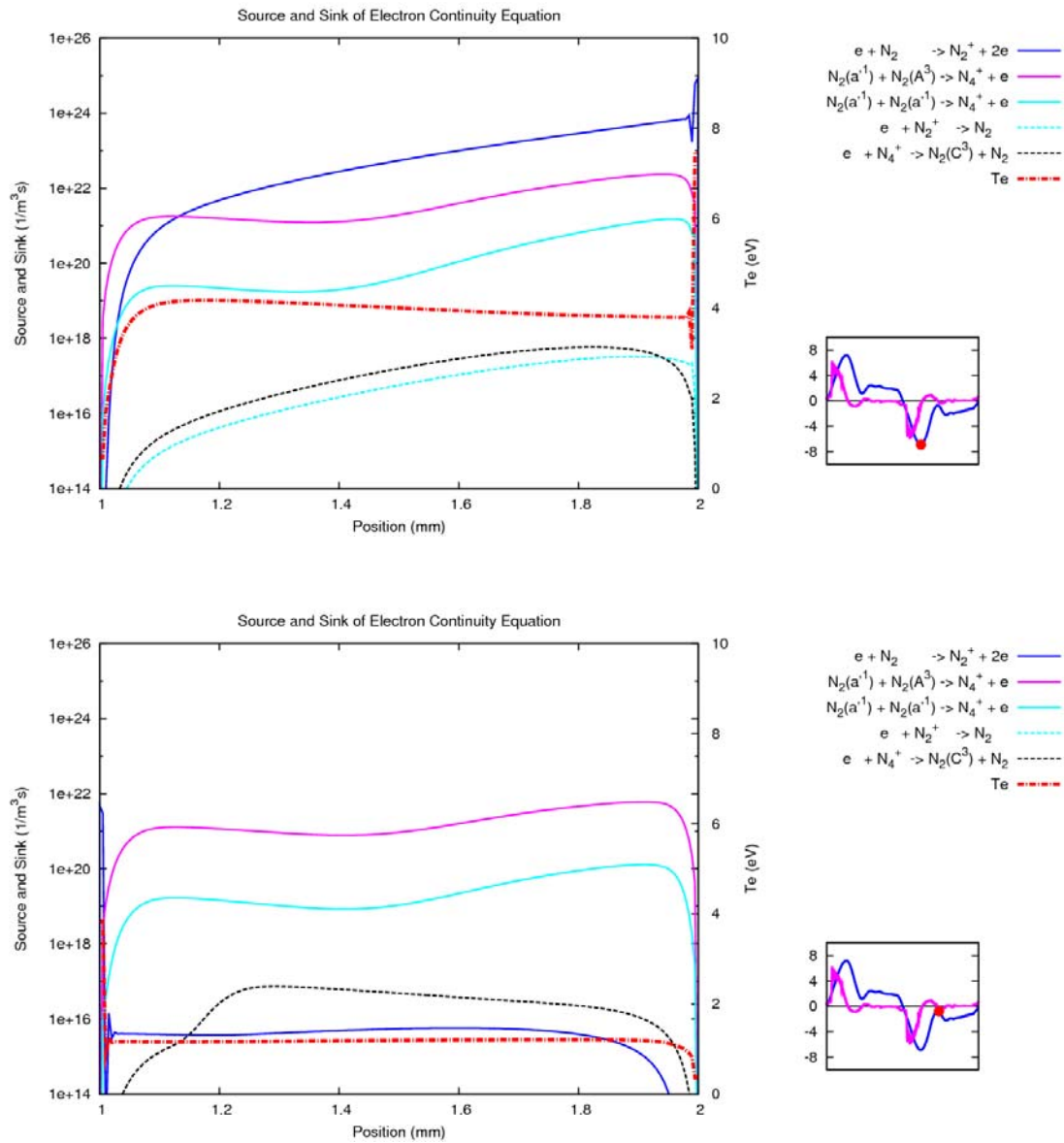


Figure 20: The source terms of electron continuity equation source terms shows in each reaction channels.



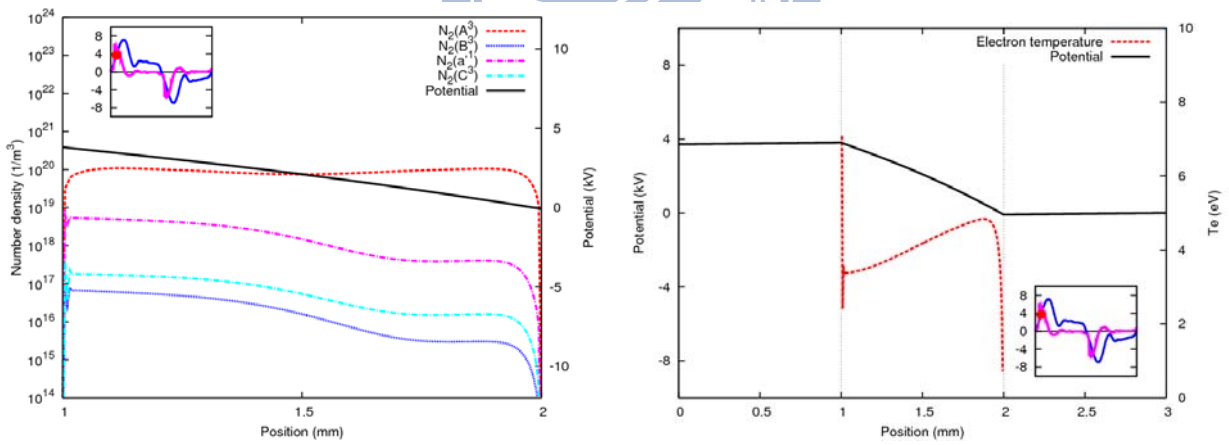
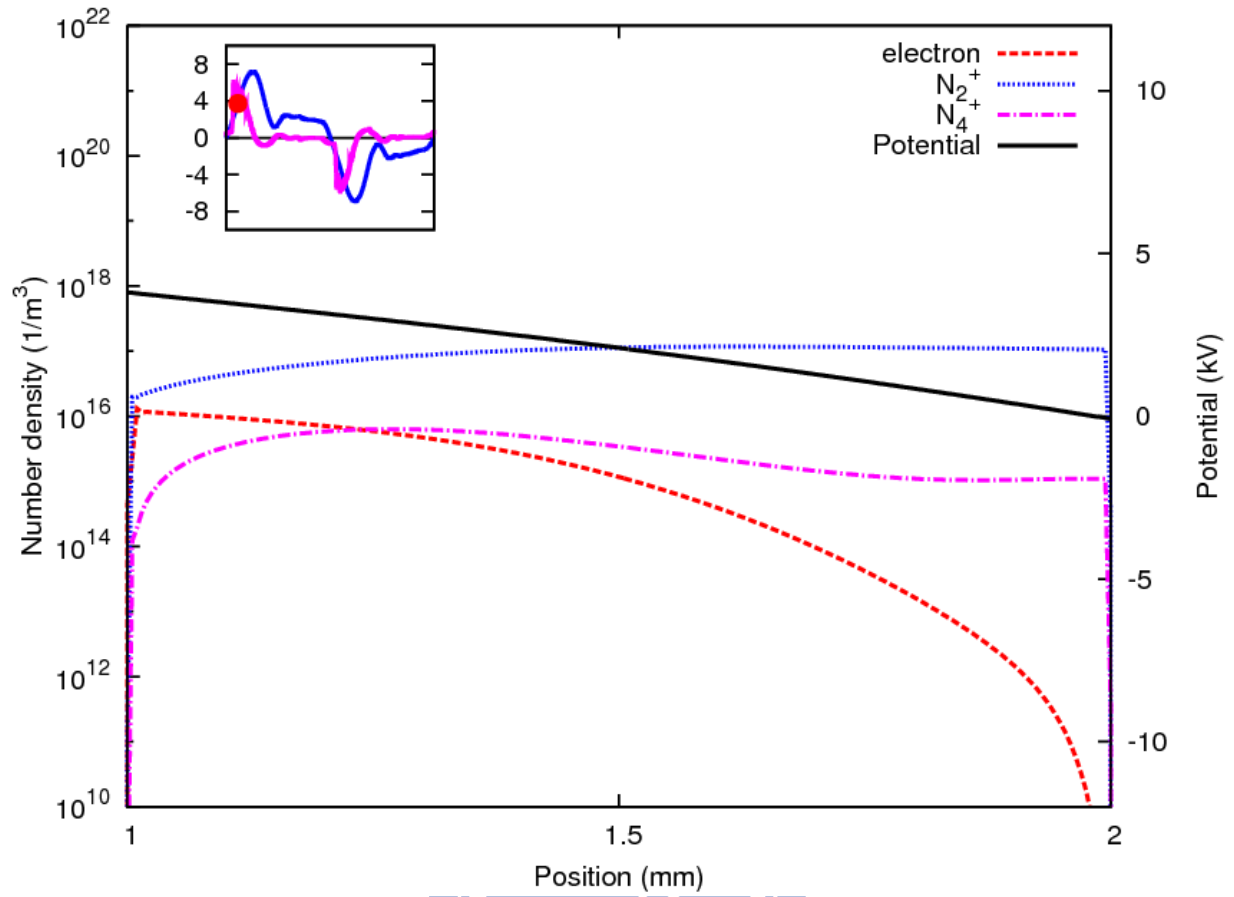


Figure 21 a

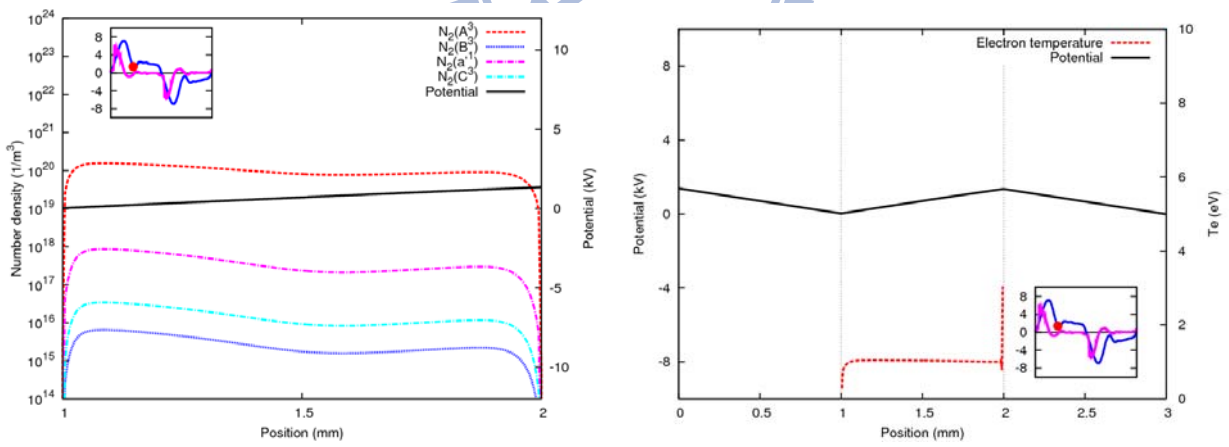
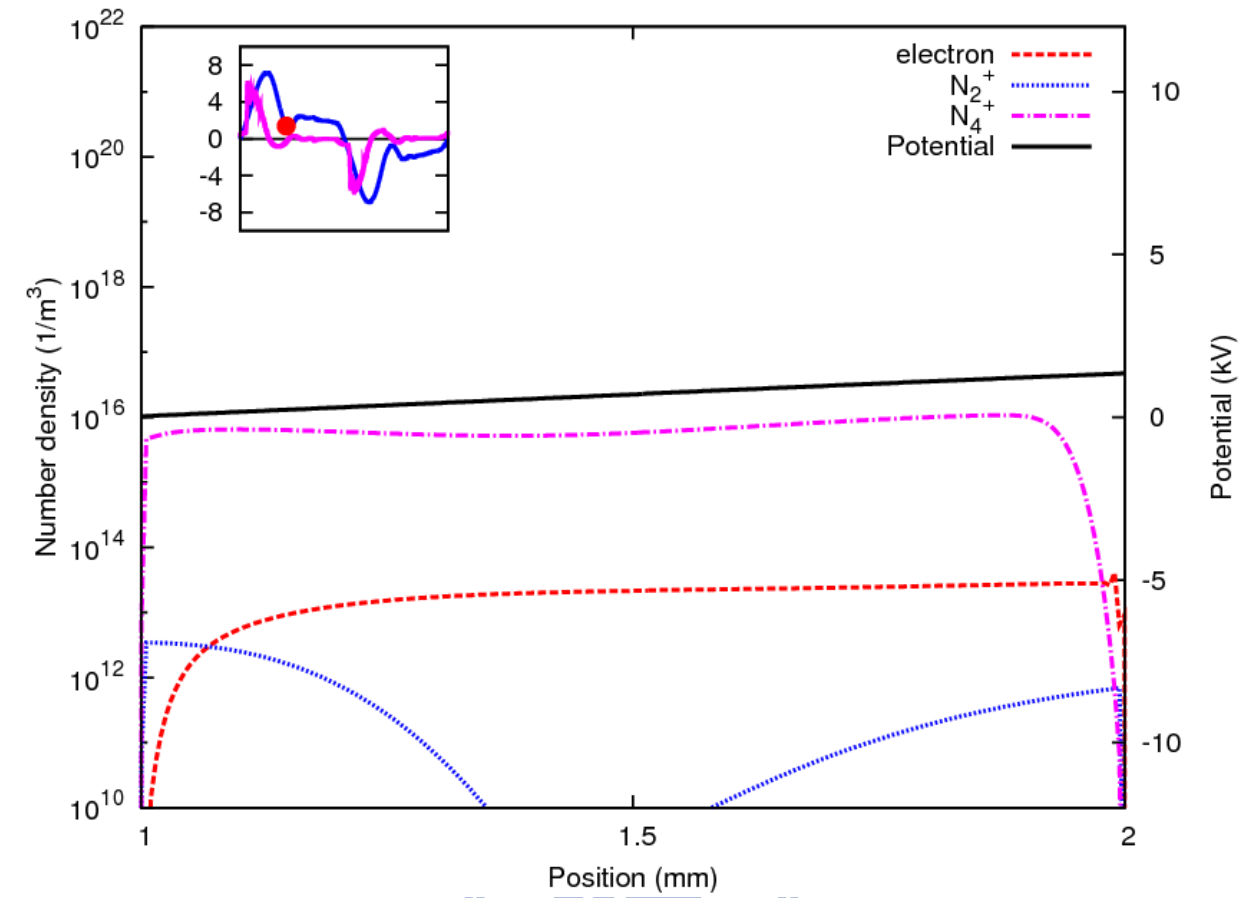


Figure 21 b

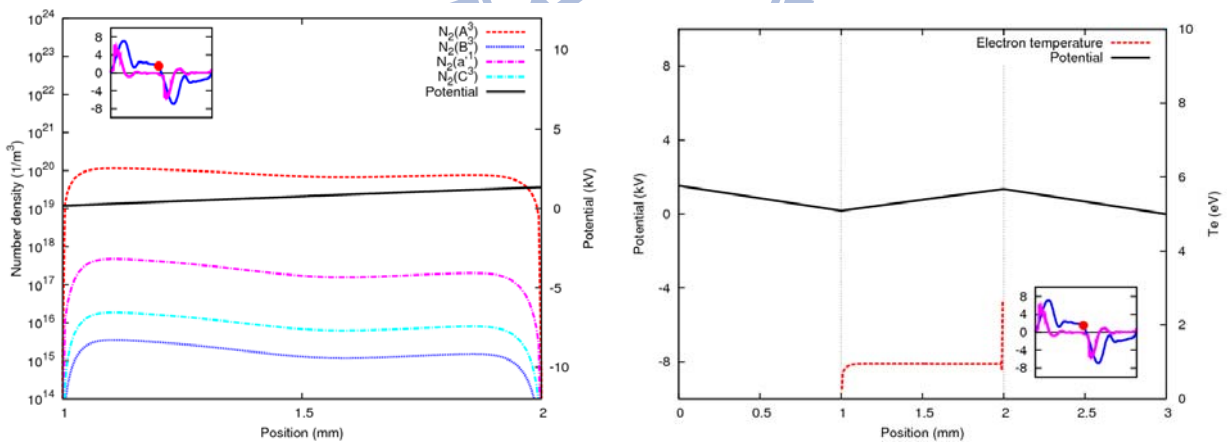
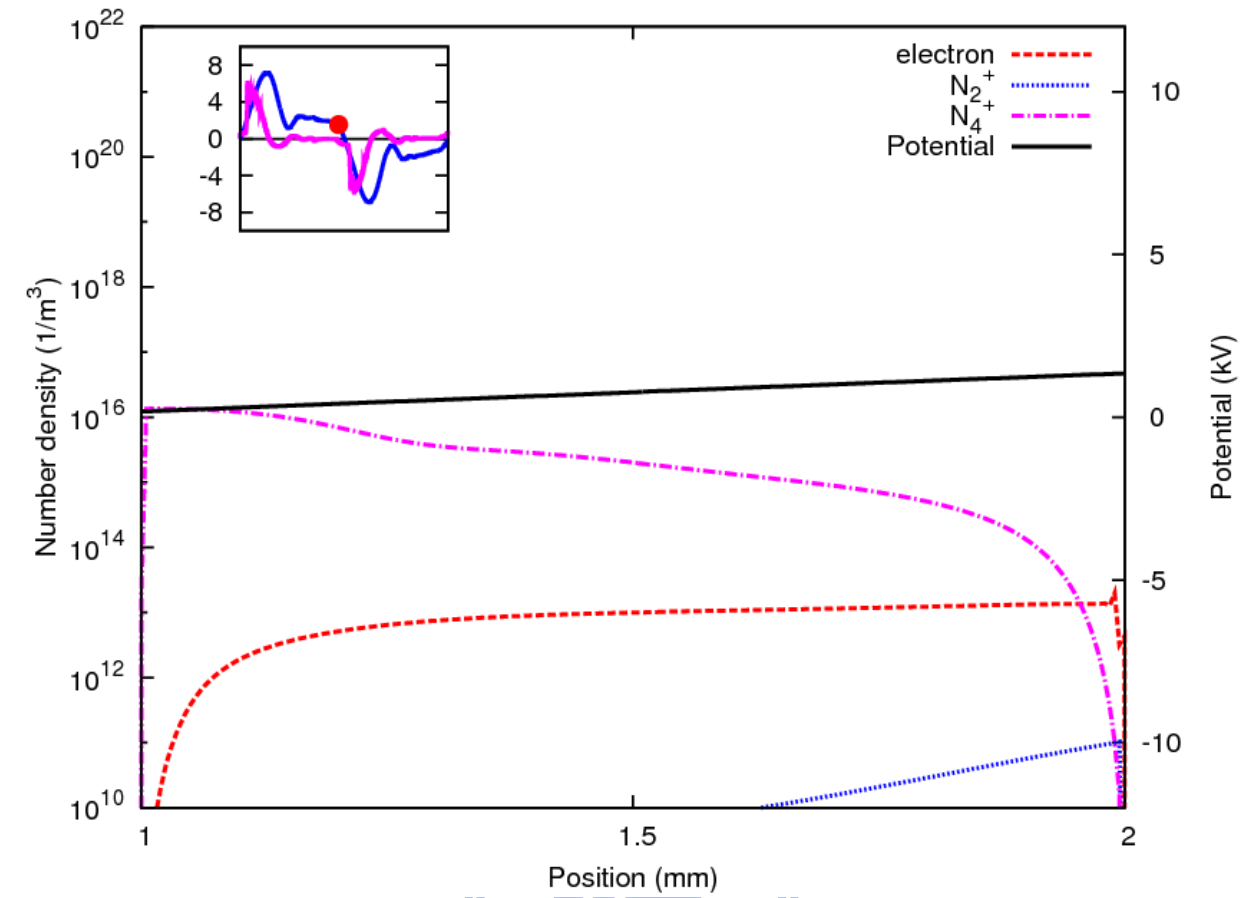


Figure 21 c

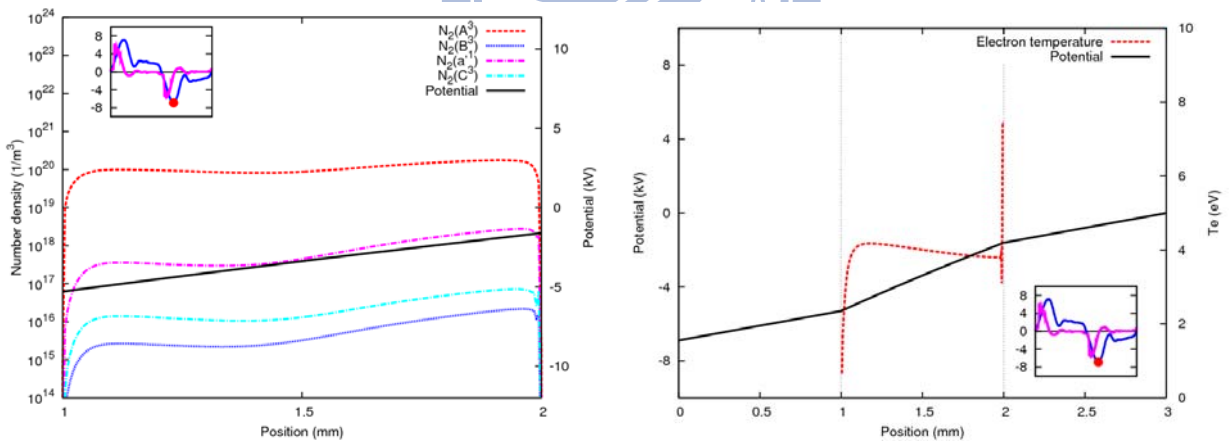
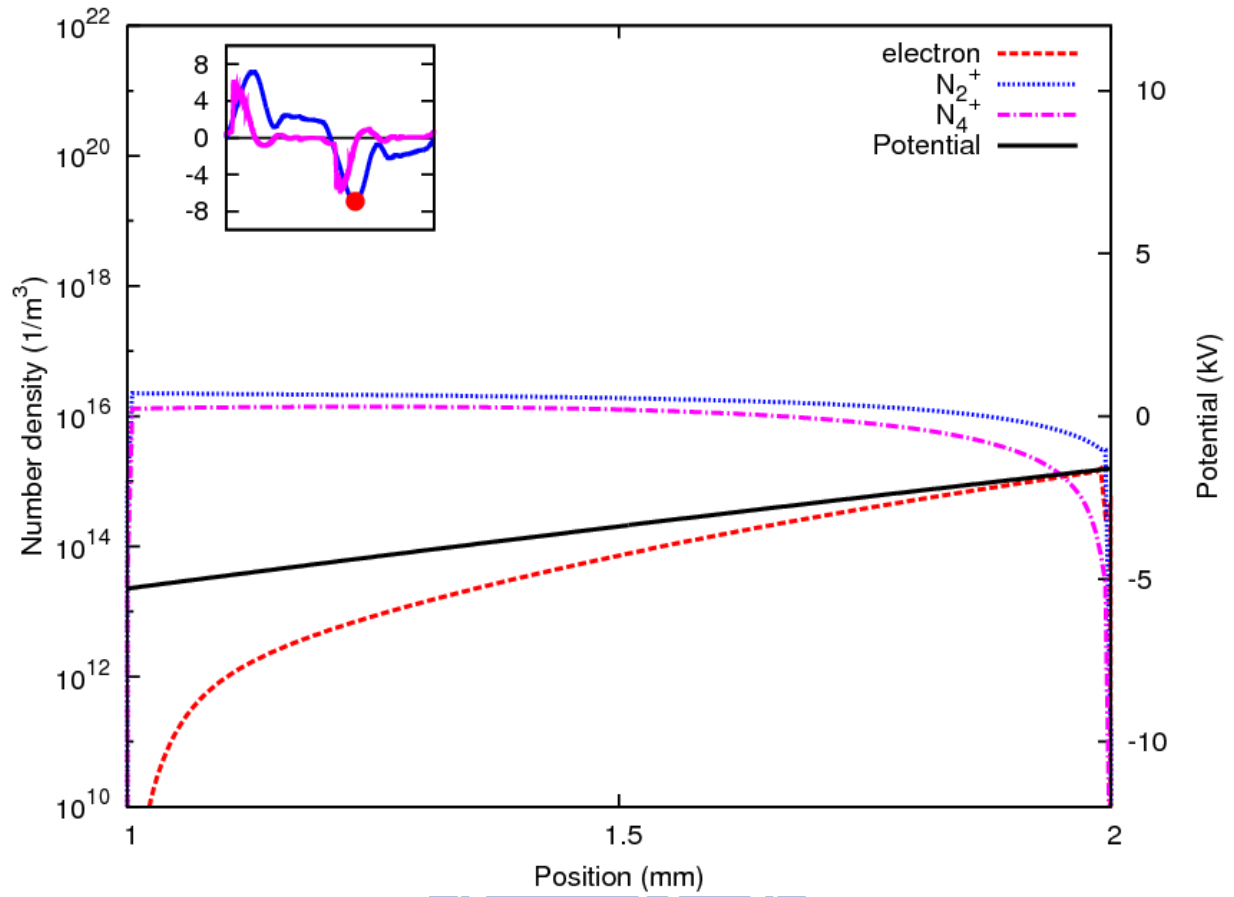


Figure 21 d

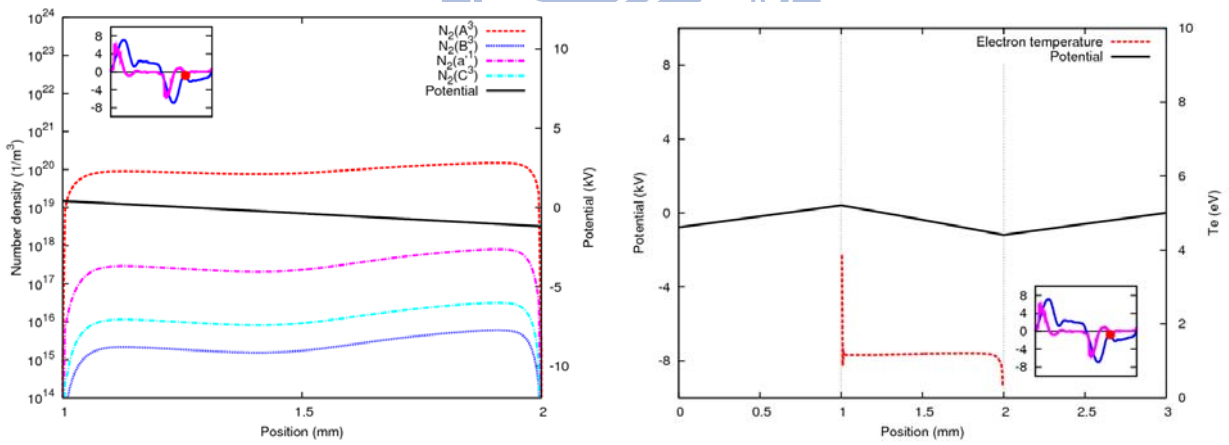
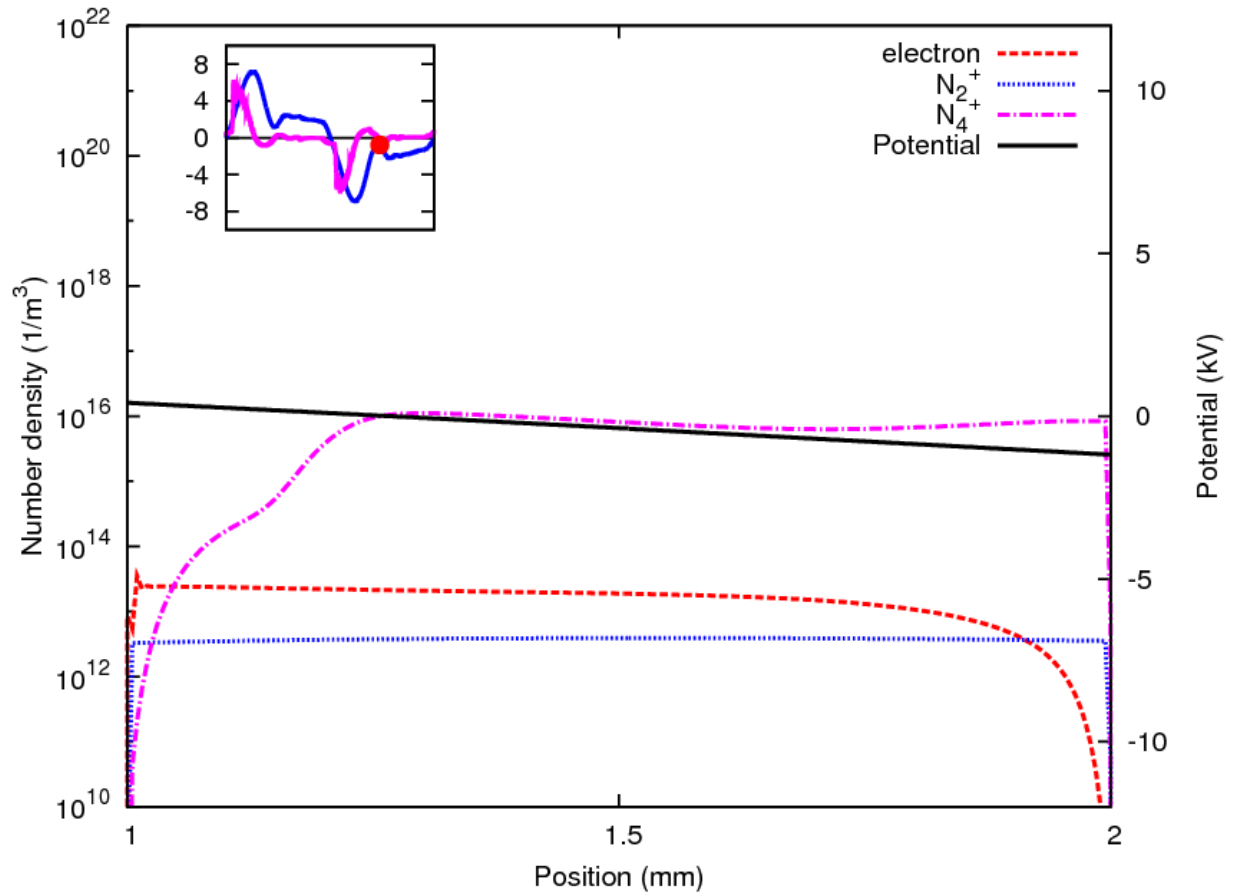


Figure 21 e

Figure 21: The sketches of potential, number density and electron temperature at different time, which from Figure 21 a to Figure 21 e, with the frequency of applied voltage 60 kHz.

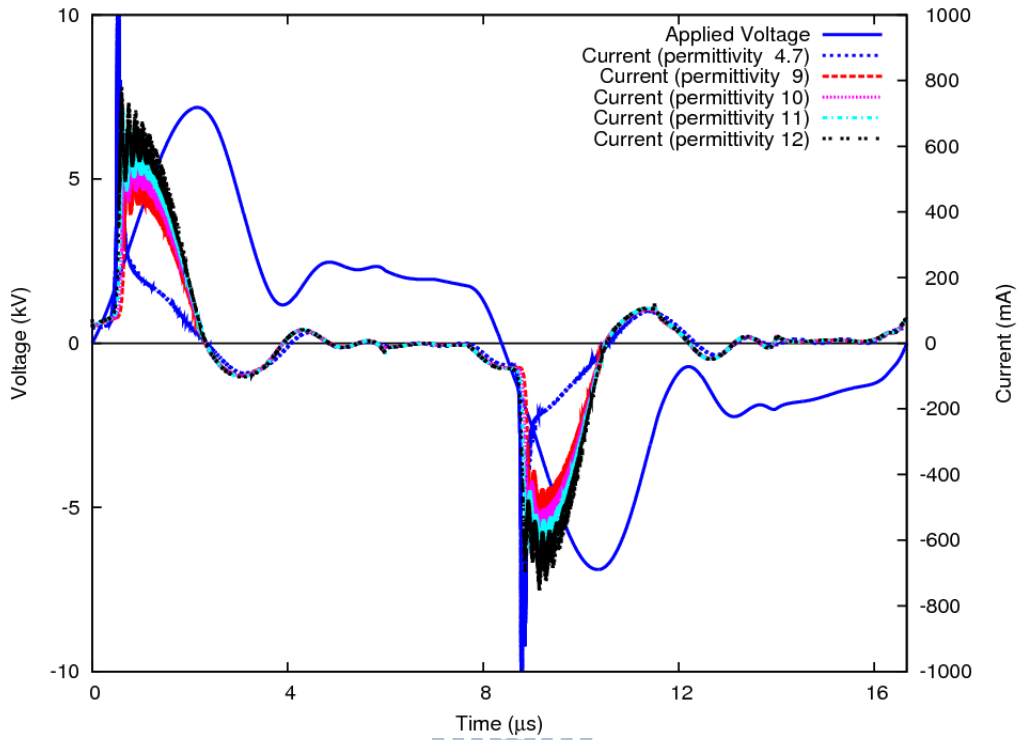


Figure 22: The total current during one cycle with the same applied voltage, gap size 1 mm and different dielectric permittivity from 9 to 12.

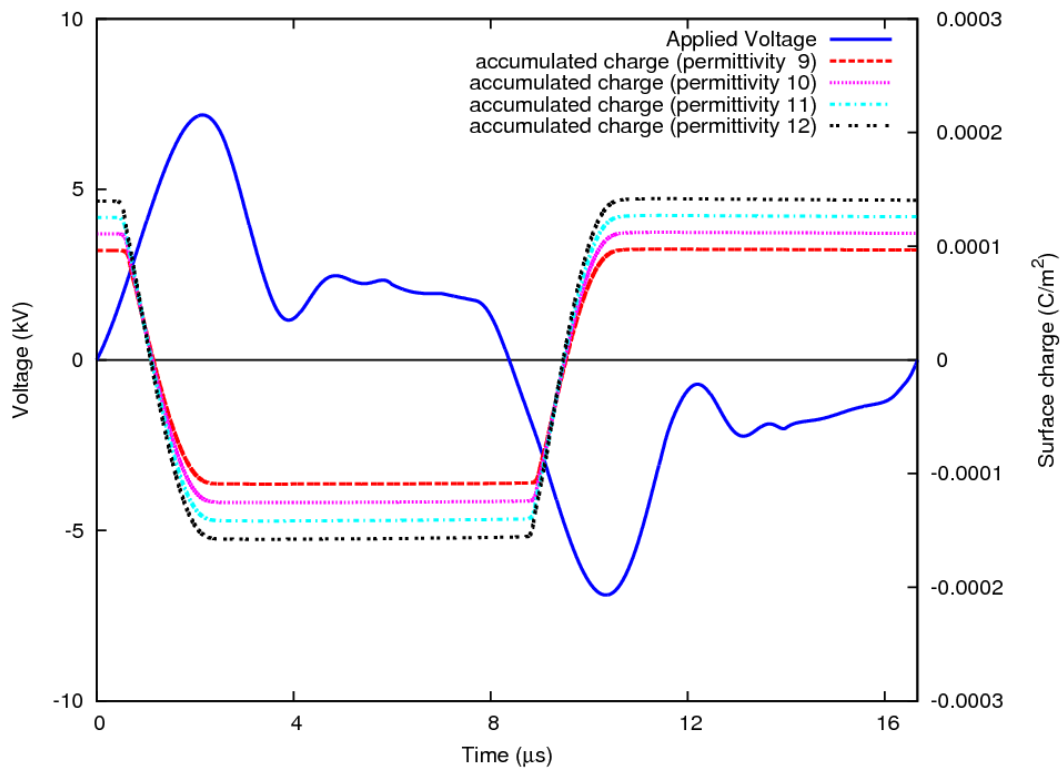


Figure 23: The accumulated charge at left dielectric surface with different dielectric permittivity, and the gap size is 1 mm with 60 kHz applied voltage.

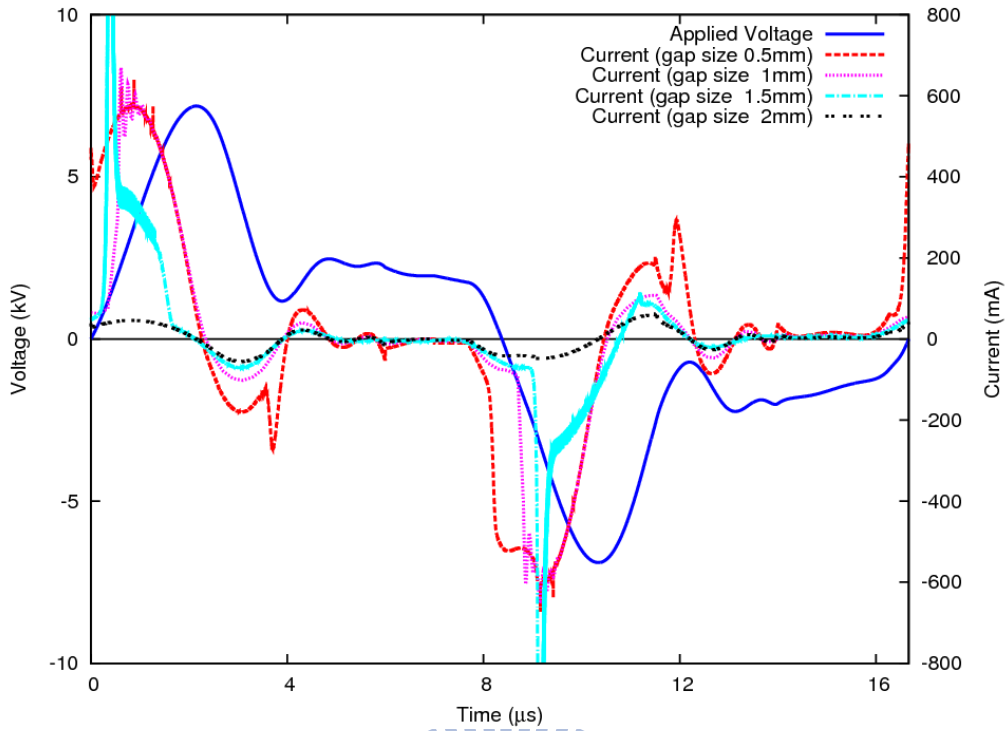


Figure 24: The total current during one cycle with the same applied voltage, dielectric permittivity 11.63 and gap size various from 0.5 mm to 2 mm.

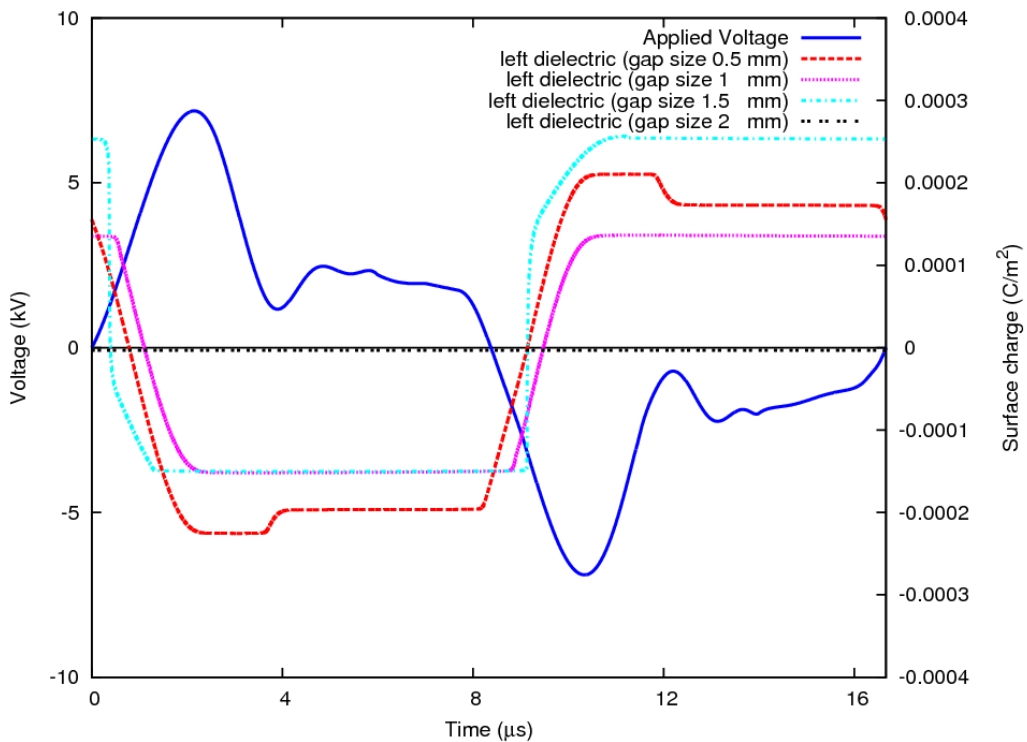


Figure 25: The accumulated charge during one cycle with the same applied voltage, dielectric permittivity 11.63 and gap size various from 0.5 mm to 2 mm.